Submitted to ApJ
Preprint typeset using LaTeX style emulateapj v. 5/2/11

arXiv:1511.06447v2 [astro-ph.HE] 28 Jan 2016

THE DEFINITIVE X-RAY LIGHT CURVE OF SWIFT J164449.3+573451

V. Mangano[1], D. N. Burrows[1], B. Sbarufatti[2,1], J. K. Cannizzo[3,4]

Submitted to ApJ

ABSTRACT

On 2011 March 28, the *Swift* Burst Alert Telescope triggered on an object that had no analog in over six years of *Swift* operations. Follow-up observations by the *Swift* X-ray Telescope (XRT) found a new, bright X-ray source covering three orders of magnitude in flux over the first few days, that was much more persistent (and variable) than gamma-ray burst afterglows. Ground-based spectroscopy found a redshift of 0.35, implying extremely high luminosity, with integrated isotropic-equivalent energy output in the X-ray band alone exceeding 10^{53} ergs in the first two weeks after discovery. Strong evidence for a collimated outflow or beamed emission was found. The observational properties of this object are unlike anything ever before observed. We interpret these unique properties as the result of emission from a relativistic jet produced in the aftermath of the tidal disruption of a main sequence star by a massive black hole (BH) in the center of the host galaxy. The source decayed slowly as the stellar remnants were accreted onto the BH, before abruptly shutting off. Here we present the definitive XRT team light curve for Swift J164449.3+573451 and discuss its implications. We show that the unabsorbed flux decayed roughly as a $t^{-1.5}$ power law up to 2012 August 17. The steep turnoff of an order of magnitude in 24 hr seems to be consistent with the shutdown of the jet as the accretion disk transitioned from a thick disk to a thin disk. *Swift* continues to monitor this source in case the jet reactivates.

Subject headings: accretion, accretion discs - black hole physics - galaxies: active - galaxies: jets - X-rays: galaxies - X-rays: individual (Swift J164449.3+573451)

1. INTRODUCTION

On 2011 March 28, the *Swift* satellite (Gehrels et al. 2004) triggered on a new source, Swift J164449.3+573451 (Swift J1644+57 hereafter). Swift J1644+57 triggered the *Swift* Burst Alert Telescope (BAT; Barthelmy et al. 2005) three more times over the next two days, a clear indication that it was not a gamma-ray burst (GRB). Observations by the *Swift* X-ray Telescope (XRT; Burrows et al. 2005) revealed an extremely variable, but previously undetected X-ray source (Burrows et al. 2011), which was found to be located at the center of a galaxy at a redshift of 0.354 (Levan et al. 2011). A consensus quickly developed that this object was a highly beamed tidal disruption event (TDE; Bloom et al. 2011; Levan et al. 2011; Burrows et al. 2011; Zauderer et al. 2011).

Because the extinction in the host galaxy is so high, the value of extinction adopted drives the inferred slope of the inherent optical-NIR portion of the spectrum, which in turn drives the interpretation of the X-ray spectrum. Burrows et al. (2011, hereafter Paper I) found that the host extinction was $A_V \approx 4.5$, which led to a positive slope of the intrinsic spectrum in the optical band and our conclusion that the optical and X-ray bands were both part of the same synchrotron component. This interpretation required that the radio emission originate in a different emission region, which we proposed was in the external shock. Zauderer et al. (2011) and Metzger et al. (2012) came to similar conclusions, based on their radio observations. Bloom et al. (2011), on the other hand, concluded that the radio and NIR/optical emission originated in the same synchrotron component.

Prior to the discovery of Swift J1644+57, relativistic jets created by tidal disruption around dormant black holes (BHs) had only rarely been discussed in the literature on TDE theory (e.g., Giannios & Metzger 2011; cf. Rees 1988; Ayal et al. 2000; Bogdanović et al. 2004; Gomboc & Čadež 2005; Brassart & Luminet 2008; Strubbe & Quataert 2009; Guillochon et al. 2009; Brassart & Luminet 2010). These earlier works generally considered scenarios in which a solar mass star is tidally disrupted by a supermassive black hole (SMBH), roughly half of the stellar mass is captured with the remainder of the disrupted star ejected into hyperbolic orbits, and visible, UV, and X-ray flares are produced by the impulsive compression of the star, the resulting accretion disk, and/or the outflowing material. In retrospect, it is not surprising that a jet could be formed in a TDE, as the SMBHs in an active galactic nucleus (AGN) produce jets under conditions of ongoing accretion. The unique aspect of this discovery was the detailed observation in the X-ray band of the turn-on of a jet in a previously dormant SMBH.

The discovery of this event produced a flurry of publications providing interpretation of the data. While most authors (including Paper I) argued for a solar mass star being tidally disrupted by a SMBH, Krolik & Piran (2011) preferred a white dwarf being disrupted by an intermediate mass BH in order to explain the rapid time variability. Cannizzo et al. (2011) suggested that the star was on an orbit with a very small impact pa-

[1] Department of Astronomy & Astrophysics, The Pennsylvania State University, 525 Davey Lab, University Park, PA 16802, USA; *vm.himawari@gmail.com*
[2] INAF – Osservatorio Astronomico di Brera, Via Bianchi 46, 23807 Merate, Italy
[3] CRESST and Astroparticle Physics Laboratory NASA/GSFC, Greenbelt, MD 20771, USA
[4] Department of Physics, University of Maryland, Baltimore County, Baltimore, MD 21250, USA

rameter, and the resulting plunge deep into the SMBH potential well totally disrupted the star, which was then completely swallowed by the BH.

The purpose of the present work is the complete analysis of the *Swift*/XRT follow-up data of Swift J1644+57 from the beginning to the end of the outburst, which occurred on 2012 August 17th, 507 days after the initial BAT trigger, and the following monitoring observations by *Swift*/XRT and *Chandra*/ACIS. We present the updated complete version of the flux light curve of the event and its analysis and interpretation.

This paper is organized as follows. In Section 2 we describe the data set. In Section 3 we describe in detail the data reduction and analysis procedures performed to obtain the final X-ray light curve of Swift J1644+57. In Sections 4 and 5 we analyze the light curve structure and late time behavior. In Section 6 we discuss our results and their implications in the context of tidal disruption models of a star by a SMBH associated to relativistic jet ejection. Finally, in Section 7 we summarize our findings and conclusions.

Throughout this paper the errors on count rates are at 1σ (e.g. in light curves; Evans et al. 2007, 2009), and the quoted uncertainties on model parameters are given at 90% confidence level for one interesting parameter (i.e., $\Delta\chi^2 = 2.71$) unless otherwise stated. Times t are referenced to the initial BAT trigger T_0 as $t = T - T_0$, unless otherwise specified. We adopt a standard cosmology model with $H_0 = 70$ km s^{-1} Mpc^{-1}, $\Omega_{\rm M} = 0.3$, $\Omega_\Lambda = 0.7$.

2. OBSERVATIONS

Swift J1644+57 triggered the *Swift*/BAT twice on 2011 March 28th, resulting in automated observations by *Swift*/XRT. It was intensively observed by *Swift* for the first four months and then was regularly monitored with single snapshots of 1 ks exposure per day, at diminishing rate per week. The whole *Swift* follow-up and monitoring campaign of Swift J1644+57 from discovery up to three years later consists of ∼700 sequences and four different trigger numbers: 450158 (seq. 0−7, from 2011 March 28 to 2011 March 30), 31955 (seq. 2-255, from 2011 March 31 to 2011 December 06), 32200 (seq. 1-237, from 2011 December 07 to 2012 August 15), and 32526 (seq. 1-200, from 2012 August 16 to 2014 March 28). The total XRT exposure in the data set is 2 Ms in Photon Counting (PC) mode and 320 ks in Windowed Timing (WT) mode (see Burrows et al. 2005, for a description of the XRT instrument modes).

We also re-analyze the 24.7 ks *Chandra*-ACIS ToO observation (PI: Tanvir), performed on 2012 November 26, and present analysis results for a second ACIS observation of 27.7 ks exposure performed by *Chandra* on 2015 February 17 (PI: Levan).

The reference time used to plot all the light curves and parameter evolution curves is the time of the first BAT trigger T_0, corresponding to T_0 = 2011 March 28 12:57:45.201 UTC = 55648.5401 MJD.

3. DATA REDUCTION AND ANALYSIS

The XRT data have been reprocessed with the HEASOFT 6.15.1 package, and the latest calibration files (version 20140610) have been used for pile-up correction and spectral response matrices production.

For light curve and hardness ratio curve extraction (see Sections 3.1 and 3.2), an annular region centered at the source position with variable inner radius has been used when pile-up correction was required, and a circular region with outer radius decreasing with the average brightness ,of the source has been used in all other cases. A minimum extraction radius of 10 pixels (23.6″) has been used starting from 2012 August 17 (day 508 since the trigger, sequence 00032526002). The background region for observations in PC mode has been selected as a set of circular regions surrounding the source where no serendipitous source was detected in the image of the summed PC observations (2 Ms exposure). The background region used for observations in WT mode in Paper I was an annular region with 65″ inner radius and 70″ outer radius. Here we preferred a constant background subtraction, with background rate estimated from average background spectra described below. This procedure allows for more reliable results, especially in the soft (highly absorbed) band 0.3−10 keV.

To extract time resolved spectra (see Section 3.3) and average spectra in or outside the light curve dips (see Section 5), source regions matching the ones used for the light curve in each corresponding time interval have been generally used. PC background spectra have been extracted from simultaneous data using an annular region centered on the source position with inner radius of 119 pixels (∼281″) and outer radius of 153 pixels (∼362″), unless otherwise stated. For the WT spectra, in order to maximize the background statistics, only two background spectra have been created: *i)* an average background spectrum (15 ks exposure) from the summed WT observations in sequences 00450158000-06, used for the early (<10 d) WT spectra; *ii)* an average background spectrum (296.5 ks exposure) from the summed WT observations in sequences 00031955014-40, used in all other cases[5]. Both background spectra have been extracted from an annular region centered on the source with 85 pixels (∼200″) inner radius and 118 pixels (∼279″) outer radius. Spectra have been generally binned to at least 20 counts per energy bin to allow for fitting in χ^2 statistics within `xspec`, unless otherwise stated. Ancillary response files were generated with the task `xrtmkarf` within HEASOFT, and account for different extraction regions and point-spread function corrections.

Chandra-ACIS data have been analyzed with the CIAO software package (v4.7), using the calibration database CALDB (v4.6.7) and standard ACIS data filtering. We used the `wavedetect` task for source detection. The source and background regions used for count rate estimation and spectral extraction are a circle centered on the source position with 1.″5 radius, and a source free annular region with 15″ inner radius and 45″ outer radius, respectively. For spectral analysis the data were binned to 1 count per energy bin to allow for fitting with Cash statistics (Cash 1979) in `xspec` (with χ^2 statistic test evaluation enabled). *Chandra* results are presented and discussed in Section 6.2.

3.1. *Count Rate Light Curve*

[5] Note that no WT observations corresponding to trigger numbers 32200 or 32526 are present in our data set.

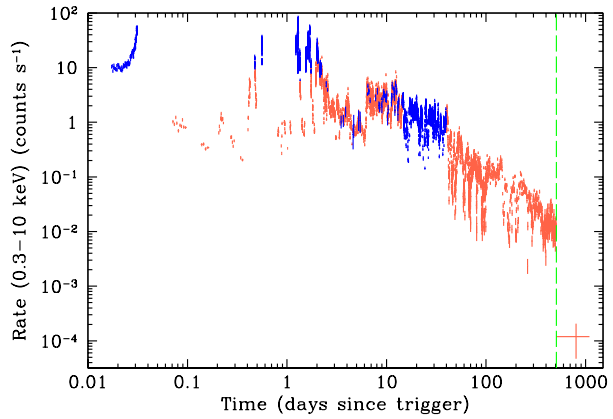

Figure 1. X-ray light curve of Swift J1644+57 in the 0.3−10 keV band. Blue points are data taken in WT mode; red points are data in PC mode. Details of the early X-ray light curve are presented and discussed in Paper I. Here we present the entire light curve measured by the *Swift*/XRT. Note the strong variability during the first three days, the decay beginning around day 7 and punctuated by deep dips at irregular intervals, and the abrupt decline on day 508 marked by the vertical dashed green line. See Figure 2 for details. The error of the late detection after the dashed green line is at the 99% confidence level.

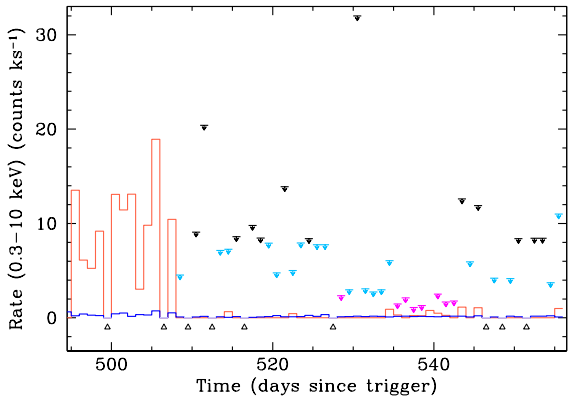

Figure 2. X-ray light curve of Swift J1644+57 in the 0.3−10 keV band during 2012 August and September, binned in days. The red histogram represents the count rate measured in the source region. The blue histogram represents the background rate rescaled to the source region area from the rate measured in the background region. Errors are not plotted for a better readability of the figure. The line of black upward triangles at the bottom of the plot indicates days in which no observation was performed. The segments marked with downward arrows are the 3σ upper limits on source count rate when the source was not detected with the `ximage` command `detect`, obtained by running the command `sosta` in the position of Swift J1644+57 with user defined source and background regions. The black arrows correspond to observations with less than 1 ks exposure, the light blue arrows to 1-3 ks exposure, and the magenta arrows to more than 3 ks exposure. The plot shows that the count rate drops abruptly on day 508 (2012 August 17) and stays below the 3σ upper limit later on.

The 0.3−10 keV count rate light curve shown in Figure 1 was produced by binning the net source counts in order to have at least 200 counts per time bin at early times, and progressively decreasing the level of required counts per bin down to at least 10 counts per bin at late times, up to sequence 00032526001, observed on 2012 August 16, 507 days after the trigger. On day 508 the source emission suddenly dropped below the detection threshold for a 1−2 ks single snapshot observation (Sbarufatti et al. 2012). A detailed plot of the abrupt drop is shown in Figure 2, where data from 2012 August and September have been binned daily. The daily count rate measured in the source region (red histogram) is compared to the expected background count rate in the source region on the same day (blue histogram). When Swift J1644+57 is not detected, the 3σ upper limit on source count rate is shown. The plot shows that the count rate drops abruptly on day 508 (2012 August 17). By comparing the count rate on day 507 and the level of the deepest upper limit we see in Figure 2 (on day 537) we can state that we had a drop of more than a factor 11 in one month, i.e. a fraction of 0.06 of the total time elapsed.

The very last point in the light curve of Figure 1 is the detection obtained from the summed 191 monitoring observations performed from 2012 August 17th (marked by the green dashed vertical line) to 2014 March 28th, for a total of 284.5 ks exposure. We extracted the source counts from a circular region of 10 pixels radius (314 pixel^2 area) and estimated the background contribution from counts found in the background region (21,143 pixel^2 area, specifically selected to avoid contamination from any field source detected in the whole PC data set) and rescaled to the source region area. We obtained 78 total counts in the source region in the 0.3−10 keV band with an estimated background of 44 counts and applied the technique of Kraft et al. (1991) to calculate the upper and lower 99% confidence limits on source counts. These correspond to an average count rate of $1.2^{+0.9}_{-0.7} \times 10^{-4}$ s^{-1}. The source is also detected on the summed image of the post-drop monitoring with the `ximage` command `sosta`, centered on the position of source with user defined source and background regions, at the level $(1.5 \pm 0.4) \times 10^{-4}$ s^{-1} with 3.8σ significance.

3.2. *Hardness Ratio*

The band ratio and hardness ratio curves of Swift J1644+57 are shown in Figure 3. We have defined the energy range 0.3−1.5 keV as the soft band (S) and the energy range 1.5−10 keV as the hard band (H). We have calculated both the ratio of the counts detected in the two bands (H/S) and the hardness ratio (H-S)/(H+S). The curves have been binned in order to have at least 500 net counts in each band up to day 507 post-trigger. For the last point (covering the time interval from day 508 to day 1096) net counts in the required bands were derived from the summed post-drop observations with the same procedure used for the count rate light curve. Errors have been estimated in the Poisson approximation (Gehrels 1986) and propagated with standard error propagation formulae. At the beginning, both curves show variations tracking the light curve flares, with the hardness rising when the average rate increases, and decaying when the average rate decreases. But later phases with different trends can be identified. We observe a hardness plateau phase from ∼2.4 to ∼16 days post-trigger, corresponding to a phase of average rate decrease (from ∼2.4 to ∼6 days) followed by a rapid rise by a factor ∼10 in ∼0.3 days and a shallow decay afterwards. After

16 days, while the average rate in the light curve goes on decaying steadily, we observe a relatively rapid (∼1 day long) drop (i.e. softening) in the hardness followed by a steep rising (i.e. hardening) phase that lasts up to ∼100 days, when a final hardness plateau phase starts. In both cases the last point represents a clearly different and much softer spectral state compared to the final trend of the curve. A comparable softness is attained only at a few light curve minima between flares (e.g. the first one at ∼0.2 days), which are minima for the band ratio and hardness ratio curves as well. If the abrupt Swift J1644+57 emission drop on day 508 is due to the turn-off of the jet (Zauderer et al. 2013), which might be likely caused by a transition to a thin disk as the accretion rate dropped below a critical value of several tens of percent of the Eddington accretion rate (Zauderer et al. 2013; Tchekhovskoy et al. 2014), then the low-level residual emission we detected later should have a different origin and this discontinuity in the hardness curves would not be surprising.

We see evidence of different spectral phases during Swift J1644+57 evolution also in Figure 4, where the soft band ratio S/(H+S) is plotted against the total rate (H+S) in the 0.3−10 keV band. Here XRT data in different operation mode are color-coded as in the previous figures, and different markers distinguish early emission (before 2.4 days, filled circles) from intermediate (between 2.4 and 39 days, empty stars) and late emission (after 39 days, empty triangles). According to this plot early data show an anti-correlation between the soft band ratio and the overall count rate i.e. a trend for harder spectra at higher rates. The correlation is tighter for WT data. PC data are more dispersed and seem to lie on a different correlation, also consistent with the harder-when-brighter trend. Late data are in PC mode only, and follow an opposite trend of harder spectra at lower rates despite the large dispersion. Intermediate data populate the central part of the plot. Part of these (WT data up to 23 days, dark blue empty stars) were included in the corresponding plot in Paper I (Supplementary Figure 4) and are interpreted as a second branch of the WT harder-when-brighter correlation after a count-rate discontinuity at ∼4 s^{-1}. The inclusion of the remaining WT data (light blue empty stars) has not completed the correlation in the left upward direction as expected, but simply thickened the data cloud on the left direction. Note that count rates as low as those reached by the WT data in Figure 1 are not seen in this plot because of the different binning criterion used. The intermediate PC data populate the bottom of the central cloud, spanning a range in rates comparable to the intermediate WT data, but with much less spread in softness (consistent with the plateau observed in Figure 3 between 2.4 and 16 days). With the possible exception of intermediate PC data, intermediate WT and late PC data in Figure 4 may be interpreted as a single component obtained by shifting leftwards and downwards with time an anti-correlation law similar to the one followed by the early WT data. This result could be obtained with a global hardening with time superimposed on a strict hardness-tracking-brightness rule on the smaller variability timescales of flares and dips.

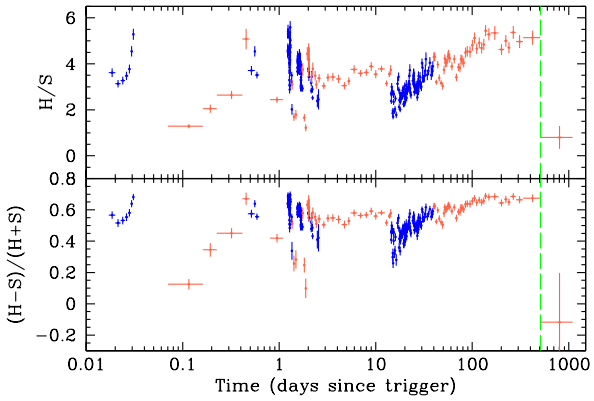

Figure 3. Top panel: X-ray band ratio curve of Swift J1644+57, calculated as the ratio of the count rate in the 1.5−10 keV band (H) to that in the 0.3−1.5 keV band (S). **Bottom panel:** hardness ratio curve (H-S)/(H+S). In both panels blue points are data taken in WT mode; red points are data in PC mode. The vertical dashed green line marks the abrupt drop in the rate light curve.

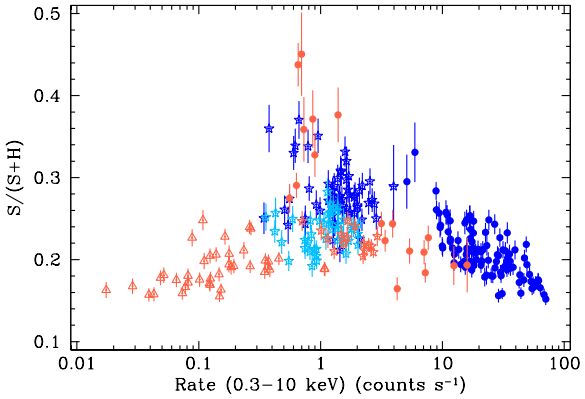

Figure 4. Soft band ratio S/(H+S) versus 0.3−10 keV rate for the light curve of Swift J1644+57. Dark blue and light blue points are data taken in WT mode, the former already presented in Paper I (up to 23 days since the trigger, Supplementary Figure 4), the latter (from 24 to 39.5 days) shown here for the first time. Red points are data in PC mode. Filled circles represent WT and PC data up to 2.4 days since the trigger; empty stars represent WT and PC data between 2.4 and 39.5 days since the trigger; empty triangles represent PC data between 39.5 and 507 days post-trigger.

3.3. *Spectral Analysis and Conversion to Flux*

The XRT team's on-line light curve repository (`http://www.swift.ac.uk/xrt_curves/00450158/`; Evans et al. 2009) uses a single conversion factor between count rate and flux (ECF), determined using an automated spectral fit of the PC mode data. This works well for GRBs, since there is rarely any significant spectral evolution after the first few ks of the afterglow, but it does not work well for Swift J1644+57, due to the extremely strong spectral variations during the first few hundred days (Figure 3). A more realistic conversion to flux can be obtained via time-dependent spectral analysis. The procedure, which we already applied in Paper I, consists of the following steps: *i)* split the

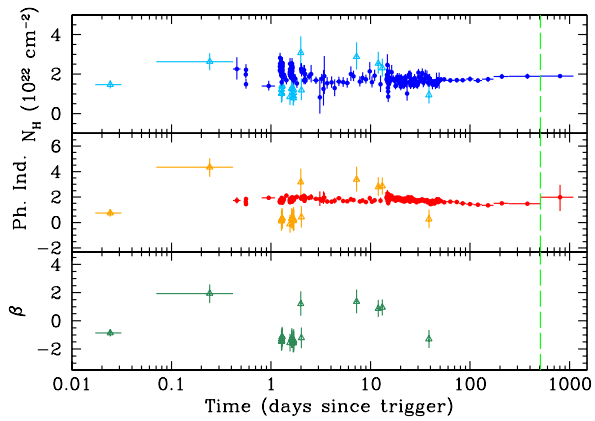

Figure 5. Temporal evolution of the best-fit parameters of the time-resolved spectra of Swift J1644+57. **Top panel:** intrinsic absorption column. **Central panel:** photon index. **Bottom panel:** curvature of the log-parabola. In all panels, filled circles represent spectra well fit by an absorbed power-law model, while open triangles are used for the 20 spectra for which the absorbed log-parabola model gives a better fit according to F-test as described in the text. The vertical dashed green line marks the drop in the count rate light curve. Remember that the photon index of the after-drop spectrum has been estimated with intrinsic N_H value fixed at 1.9×10^{22} cm^{-2}.

data set into a sequence of short time intervals tracking the hardness states of the source but with enough counting statistics to use standard χ^2 fitting techniques, and extract spectra for each time interval; *ii)* fit each spectrum, derive the ECF corresponding to the best-fit model, and create a stepped ECF evolution law; *iii)* convert the count rate light curve to flux by applying at each point an ECF obtained through a cubic spline interpolation of the ECF stepped curve.

The conversion applied in Paper I was limited to the first 50 days of the Swift J1644+57 outburst, and was based on spectral modeling with the log-parabola model defined as $A(E) = E^{(-\alpha+\beta\log_{10}(E))}$ where α is the photon index and β is a measure of the curvature compared to a simple power law, which is obtained for $\beta = 0$. The complete spectral model we use also includes two absorption components: a Galactic one with N_{Hgal} fixed to 1.7 $\times$ 10^{20} cm^{-2} (Kalberla et al. 2005) and an intrinsic one at redshift $z = 0.35$ with N_H allowed to vary with time. The log-parabola model has been introduced as a good empirical fit for broadband spectral distributions of BL Lacs and other blazar sources. The version we use corresponds to the model `logpar` in `xspec` (Massaro et al. 2004) with (constant) parameter pivot-E (representing the low end of the energy range used in the fit) fixed to 1 keV, and curvature parameter equal to $-\beta$. In Paper I we reported that the log-parabola spectral model generally provided better fits than a simple power law to both time and intensity-selected spectra of Swift J1644+57, though power-law fits were statistically acceptable. However, in about 74% of cases the best-fit value of the parameter β was consistent with zero within its uncertainties, making the model perfectly equivalent to a power law (see Supplementary Figure 11 in Paper I), but with substantially larger errors on both the intrinsic absorption column and the photon index compared to the power-law fit.

For the present paper, we complete the set of time-dependent spectra used in Paper I with more spectra extracted from the data collected after the first 50 days and before the light curve drop, reaching a total of 215 spectra (163 in WT mode and 52 in PC mode). We have reanalyzed the whole data set with updated spectral response files, fitting each spectrum with both power-law and log-parabola models[6]. Since these two models are suitable for an F-test (Protassov et al. 2002), we apply it to estimate the probability P of chance improvement of the χ^2 and reject all the log-parabola fits with P $>$ 0.01. This condition rejects 195 of the log-parabola fits (including all the best-fit solutions with β consistent with zero within errors) i.e., according to this selection the log-parabola model significantly improves the fit only for 20 spectra (15 in WT mode and 5 in PC mode). Thus, for every further calculation, we decided to use the power-law fit results for all the spectra but the 20 for which the log-parabola fit represents a significant improvement.

We also extracted and analyzed a spectrum from the summed PC data collected after the drop in the light curve, choosing source and background extraction regions as we did for the final count rate and hardness ratio calculation. In this case the data were binned to 1 count per energy bin to allow for fitting with Cash statistics (Cash 1979) in `xspec` (with χ^2 statistic test evaluation enabled). The very low statistics do not allow for a fit with an absorbed power-law with both intrinsic N_H and photon index free or an absorbed log-parabola model in this case. We modeled the spectrum with an absorbed power-law with intrinsic N_H fixed to 1.9×10^{22} cm^{-2}. The best fit photon index is $\Gamma = 2 \pm 1$. The fit is poor and the uncertainty is very large. Γ values larger than 2 are likely to be preferred because corresponding models give H/S $<$ 1.5. The correct band ratio may be achieved also with Γ values smaller than 2 and lower intrinsic N_H. We then performed a second fit with Γ fixed to 1 and free intrinsic N_H. The fit is apparently equivalent to the previous one and formally gives $N_H < 0.5 \times 10^{22}$ cm^{-2}, but the model cannot reproduce an $H/S \sim 1$ unless N_H is zero.

Our final best-fit results, including those for the post-drop spectrum, are listed in Table 1 and shown in Figure 5. The log-parabola model is a curved model with a broad minimum in the spectrum at $E_{crit} = 10^{(\alpha-2)\frac{2}{\beta}}$ keV if $\beta > 0$, or a broad peak at energy E_{crit} for $\beta < 0$. Note that among the log-parabola best-fit models that survive our selection, we have five with positive values of β and all of them correspond to PC spectra. In all cases E_{crit} is in the 2.5$-$6.0 keV range, well within the *Swift*/XRT energy band, but the peak/minimum is so broad compared to the band (relative width $\sim |\alpha/\beta|$) that almost no curvature can be seen by eye in the spectrum. Finally, the 20 log-parabola fits show a strong correlation between N_H, photon index, and β. This is apparently unrelated to any physical status, because the 20 spectra do not show any common property (e.g. corresponding to peaks or minima, showing pile-up, etc.). We are led to believe that in these 20 special cases the log-parabola fits are merely approximate descriptions that we cannot

[6] With the exception of the post-drop spectrum, where low statistics did not allow us to fit the log-parabola model.

Table 1
Swift J1644+57: Best Fit Parameters of Time-resolved Spectra.

Number	XRT Mode	Start (days)[a]	Stop (days)[b]	N_H (cgs)[c]	Photon Index[d]	β	χ^2	dof
1	WT	0.01713861	0.03135739	$1.5^{+0.2}_{-0.2}$	$0.74^{+0.30}_{-0.28}$	$-0.86^{+0.25}_{-0.24}$	469.530	470
2	PC	0.07028800	0.41441000	$2.6^{+0.4}_{-0.4}$	$4.34^{+0.71}_{-0.74}$	$1.94^{+0.65}_{-0.69}$	131.768	104
3	PC	0.41559230	0.49312770	$2.3^{+0.6}_{-0.5}$	$1.73^{+0.25}_{-0.24}$	–	45.600	40
4	WT	0.55755144	0.55925056	$2.0^{+0.2}_{-0.2}$	$1.63^{+0.10}_{-0.10}$	–	145.590	138
216[e]	PC	508.39513700	1096.00273100	$1.9^{+0.0}_{-0.0}$	$1.98^{+0.97}_{-1.08}$	–	23.611	**47**

Note. — This table is published in its entirety in the electronic edition of the Astrophysical Journal. A portion is shown here for guidance regarding its form and content.

[a]Starting time of data interval, relative to the first BAT trigger at T_0 = 2011 March 28 12:57:45.201 UTC = 55648.5401 MJD.
[b]Ending time of data interval, relative to the first BAT trigger at T_0 = 2011 March 28 12:57:45.201 UTC = 55648.5401 MJD.
[c]Units are 10^{22} cm^{-2}.
[d]Gives the value of the parameter α when the value of β is listed.
[e]Spectrum of the post-drop phase.

use for any other purpose than flux estimation.

The ECFs to be used for the final conversion from count rate (Figure 1) to 0.3−10 keV observed flux are derived from the best-fit results listed in Table 1 and are shown in the left panel of Figure 6, while in the right panel of the same figure we show the corresponding ECFs for conversion into 0.3−10 keV unabsorbed flux. Note that in this latter case the five log-parabola best-fit models with $\beta > 0$ lead to higher than average values of the ECF, and all those with $\beta < 0$ lead to lower than average values of the ECFs. This is due to log-parabola spectra with $\beta > 0$ having larger than average N_H values and softer than average photon indices, as opposed to the $\beta < 0$ solutions, for which the opposite is true. The correction for the absorption leads to a larger scatter in the ECFs. The absolute average deviation of the ECFs (i.e. the average of their differences from the mean value, taken in absolute value) rises from 7% to 15% of the mean value going from the left panel to the right panel in Figure 6.

The final light curve in observed and unabsorbed flux will be introduced and discussed in Section 3.4. Note that the ECFs for the observed flux after day 15 change systematically, mirroring the strong variations in the band and hardness ratio plots of Figure 3. This could lead to a different slope for the overall decay rate than would be obtained using a single mean ECF. The ECFs for the unabsorbed flux, instead, show an average constant trend after day 15, in better agreement with the standard XRT light curve repository.

A closer look at the temporal evolution of the spectral parameters in Figure 5 shows that the variations of both the intrinsic N_H and the photon index approximately track the rate, but with opposite trends: the N_H tends to be higher at higher rates, while the photon index tends to be lower at higher rates, at least for the early portions of the light curve[7]. These different behaviors are visible in Figure 7, where the photon indices and the intrinsic absorption columns of the time-resolved spectra of Swift J1644+57 well fit by an absorbed power-law model are plotted as a function of the 2−10 keV flux. The photon index plot (left panel) shows a structure similar to the soft band ratio versus rate plot in Figure 4, though a larger dispersion in the different groups of data is clearly seen. The intrinsic N_H plot (right panel) has a different structure, with early data (filled circles) showing a more-absorbed-when-brighter trend, and late data (empty triangles) suggesting a moderately increasing absorption as the flux decays. The intermediate data (empty stars) are more difficult to interpret because of the large dispersion, but seem to follow a trend similar to early data. A general trend of intrinsic N_H decreasing with time is confirmed by a linear fit of N_H versus $\log_{10} t$. With t in units of days we obtain an intercept at 1 day of $(1.98\pm0.02)\times10^{22}$ cm^{-2} and a linear coefficient of -0.44±0.02, with a χ^2_r =1.522 (213 dof). An analogous fit for the photon index gives an intercept at 1 day of 1.82±0.01 and a linear coefficient of -0.40±0.01, with a χ^2_r =1.885 (213 dof), and confirms the general trend for hardening of the spectra we already noted in Section 3.2.

3.4. *X-ray Flux Light Curve*

The final light curves of Swift J1644+57 in observed flux and unabsorbed flux are shown in Figure 8. The conversion procedure and the time-dependent ECFs used are described in Section 3.3. Note that discrepancies between the two curves are largest in the time intervals from 0.07 days after the BAT trigger to ∼0.5 days, and from 6 to 15 days. The overall later decay does not seem dramatically affected by the correction for the absorption. Models of TDEs give predictions about the decay of the intrinsic luminosity of the source. For this reason the unabsorbed flux light curve of Swift J1644+57 should be used in testing models. This one is shown alone in Figure 9 and listed in Table 2.

The X-ray light curve of Swift J1644+57 differs from the typical X-ray afterglow light curve of a GRB in many respects. In Figure 10 we compare the X-ray light curve of Swift J1644+57 to that of GRB 060729, the longest GRB X-ray light curve ever obtained (Grupe et al. 2010).

Both curves are shown in terms of the X-ray luminosity, $L_{X,iso}$, calculated assuming isotropic emission, and are plotted in the source rest frame.

The $L_{X,iso}$ light curve of GRB 060729 has a canonical afterglow shape, with a flat plateau phase followed

[7] Note that statistical correlation between N_H and photon index in fits goes in the direction of higher N_H at higher photon index, and cannot be responsible for the observed trends with rate.

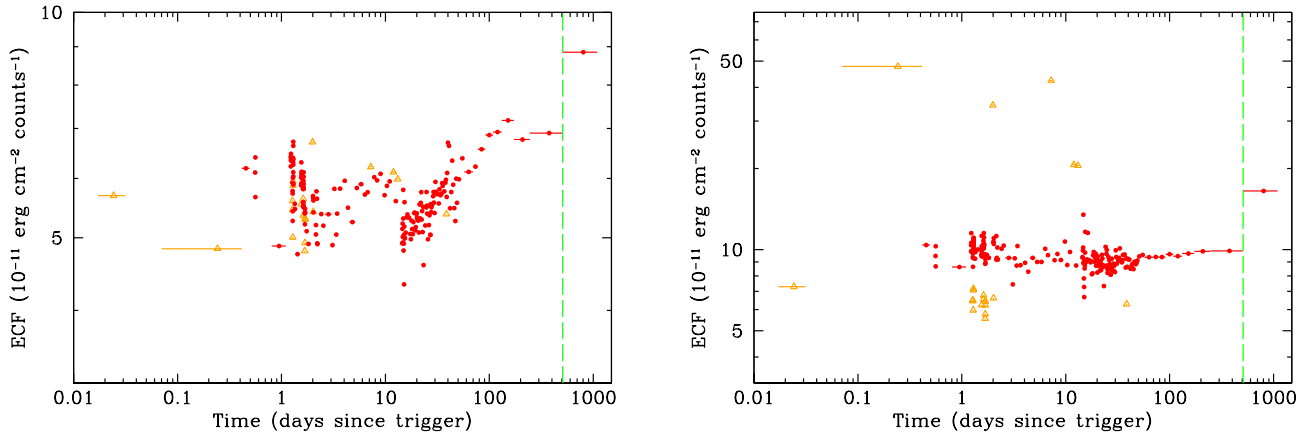

Figure 6. Left panel: Energy Conversion Factors (ECFs) used to convert the count rate light curve in Figure 1 to observed flux units. Orange triangles represent ECFs coming from absorbed log-parabola fits, and red circles represent ECFs coming from absorbed power-law fits. The vertical dashed green line marks the drop in the rate light curve. The variations in the ECFs mirror the strong variations in the band and hardness ratio plots of Figure 3. **Right panel:** Energy Conversion Factors (ECFs) to be used for conversion of the count-rate light curve of Swift J1644+57 into unabsorbed 0.3−10 keV flux. Symbols and colors are as in the left panel.

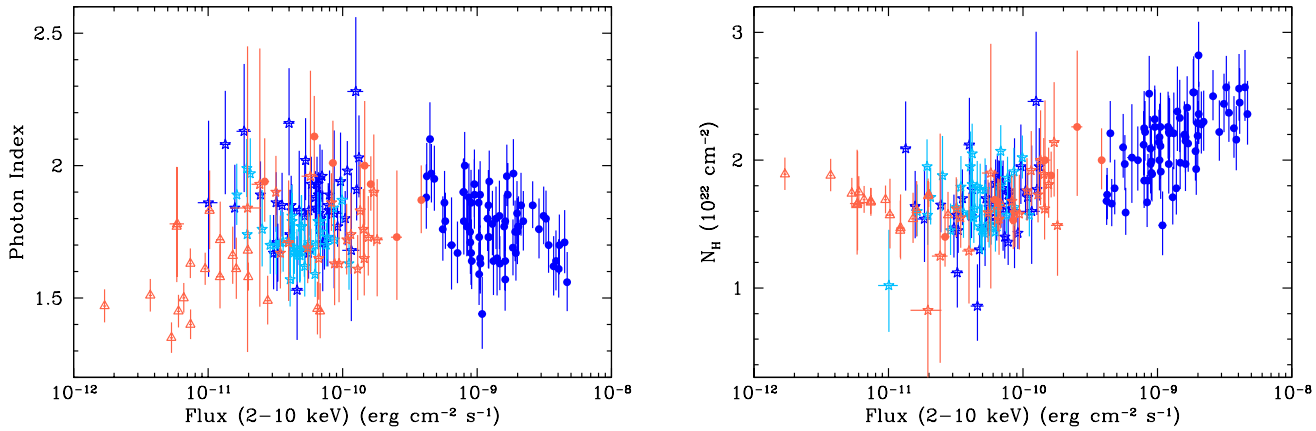

Figure 7. Left panel: photon indices of the time-resolved spectra of Swift J1644+57 well fit by an absorbed power-law model as a function of the 2−10 keV flux. **Right panel:** intrinsic absorption column N_H as function of the 2−10 keV flux for the same spectra used in the left panel. In both panels colors and symbols are defined as in Figure 4.

by a power-law decay similar to the late average decay of Swift J1644+57, but starting about 30 times earlier and running three orders of magnitude below the Swift J1644+57 light curve for $t > 10$ days. As illustrated by GRB 060729, GRB afterglows are typically fairly smooth; they may show flares (usually in the first day, before and/or during the plateau phase) but never show dips, nor has a GRB ever exhibited a range of variability like that seen in Swift J1644+57, which uniformly spans more than one order of magnitude throughout its evolution. Moreover, GRB afterglows rarely exhibit spectral evolution after the first day, while we have shown that Swift J1644+57 exhibits strong spectral evolution for well over a year.

The overall shape of the X-ray light curve of Swift J1644+57 also differs from typical X-ray light curves from long-term monitoring of blazars, the class of AGN sources with observed radiation dominated by the emission from relativistic jets pointing at the observer. The typical dynamic range of blazar flares in X-rays is a factor of a few, not several orders of magnitude, and the typical activity duty cycle is small compared to that of the initial flares of Swift J1644+57 (Krolik & Piran 2011).

4. LIGHT CURVE DECAY

The X-ray light curve of Swift J1644+57 is highly variable and affected by bright flares and deep dips at irregular intervals throughout the whole XRT monitoring, but overall, there appears to be a continuous trend underlying the flaring and dipping activity in the light curve starting about 6 days after the trigger. The upper envelope appears to follow a steady power-law decay from about ∼6 days post-trigger to the end of the outburst. The modeling of this global trend is important for the interpretation of the phenomenon. In order to do it, we

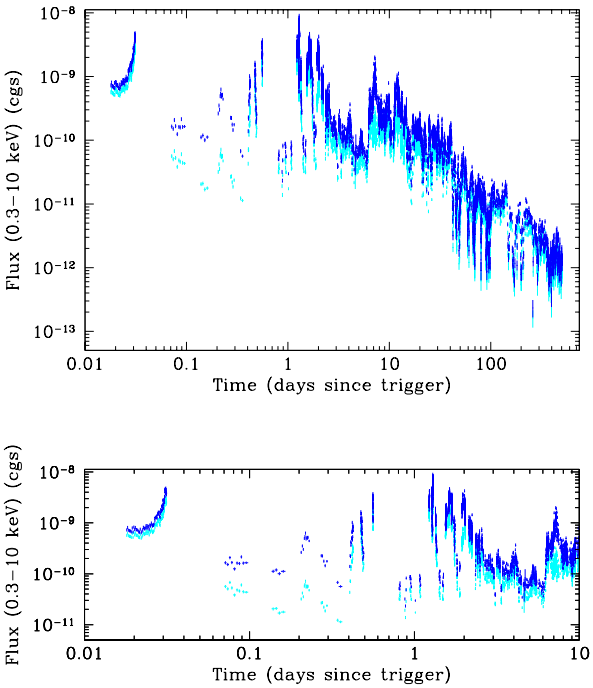

Figure 8. Top panel: X-ray flux light curves of Swift J1644+57 in the 0.3−10 keV band obtained with the time-dependent conversion procedure described in Section 3.3 applied to the two sets of ECFs from Figure 6. The curve in observed flux is colored in light blue and the one in unabsorbed flux is in blue. **Bottom panel:** detail of the first 10 days of the flux light curves of Swift J1644+57. Color coding as in the top panel.

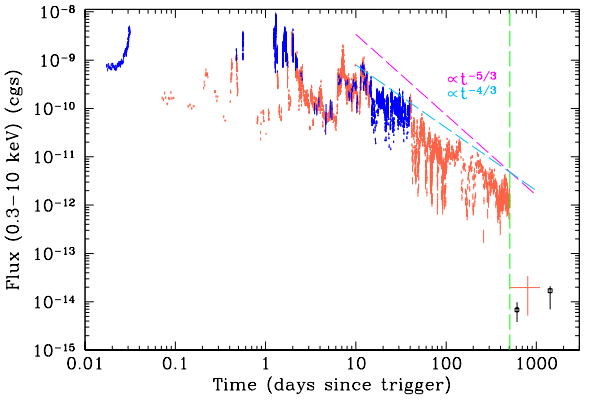

Figure 9. X-ray flux light curve of Swift J1644+57 in the 0.3−10 keV band, unabsorbed. The XRT operation modes are color coded as in Figure 1: blue for WT mode and red for PC mode. The vertical green dashed line marks the sudden drop of 2012 August 17. The open black squares mark the two *Chandra*-ACIS observations performed on 2012 November 26 and 2015 February 17 (see Section 2). For comparison, we show decay rates of $t^{-5/3}$ and $t^{-4/3}$ measured relative to the BAT trigger time.

proceeded as follows:
(1) we generated a set of six progressively smoothed light curves by rebinning the unabsorbed flux light curve computed in Section 3.4 using a decreasing number of time

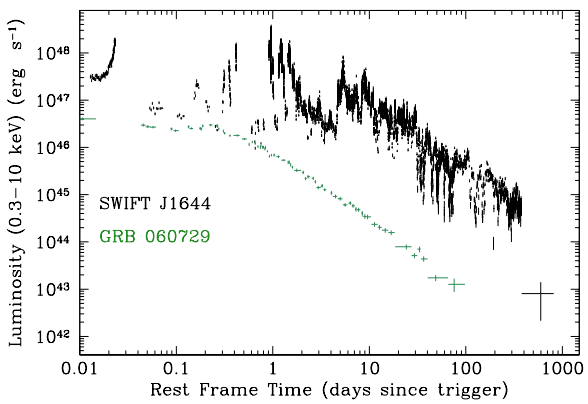

Figure 10. X-ray isotropic luminosity, $L_{\rm X,iso}$, of Swift J1644+57 in the 0.3−10 keV band, compared to the isotropic luminosity of GRB 060729, a long-lived but otherwise typical GRB afterglow at $z = 0.54$. No k-correction was performed, so the energy bands being compared are in the observed frame, but the difference in redshift is small (0.354 vs. 0.54).

Table 2
Swift J1644+57 X-Ray Light Curve.

t1[a] (days)	t2[b] (days)	Flux[c] (cgs)	Flux Uncertainty[c] (cgs)	XRT Mode
0.01720060	0.01742560	7.545e-10	5.449e-11	WT
0.01742561	0.01764019	7.904e-10	5.576e-11	WT
0.01764023	0.01790898	6.321e-10	4.634e-11	WT
0.01790898	0.01814023	7.300e-10	5.288e-11	WT
0.01814019	0.01835061	8.105e-10	5.702e-11	WT
0.07034943	0.07260637	1.648e-10	1.166e-11	PC
0.07260642	0.07512378	1.519e-10	1.074e-11	PC
0.07512371	0.07700449	2.083e-10	1.473e-11	PC
0.07700449	0.07940611	1.671e-10	1.181e-11	PC
0.07940616	0.08276264	1.249e-10	8.783e-12	PC

Note. — This table is published in its entirety in the electronic edition of the Astrophysical Journal. A portion is shown here for guidance regarding its form and content.

[a]Starting time of data interval, relative to the first BAT trigger at T_0 = 2011 March 28 12:57:45.201 UTC = 55648.5401 MJD.
[b]Ending time of data interval, relative to the first BAT trigger at T_0 = 2011 March 28 12:57:45.201 UTC = 55648.5401 MJD.
[c]Units are erg cm^{-2} s^{-1}.

intervals per decade of days, uniformly spaced in $\log(t)$, according to the sequence 32, 16, 8, 4, 3, and 2 intervals per decade (see Fig 11). For each time interval we calculated a rebinned point with time and flux coordinates obtained from the arithmetic averages of the logarithms of the times ($\log_{10}(t)$) and the fluxes ($f_{\rm X}$) of all the data points therein. No error estimate through error propagation has been performed because errors of the single data points are negligible compared to the dispersion of the points.
(2) we fit each smoothed light curve segment between 6 and 508 days post-trigger with a linear model in the $\log_{10}(t) - \log_{10}(f_{\rm X})$ plane (i.e., $\log_{10}(f_{\rm X}) = q - s\,\log_{10}(t)$) and derived the best-fit value of the slope s as a function of the number of rebinned points.
(3) we calculated the mean and sample variance of the

six values of s obtained in *(2)* and used the result as a measure of the average slope of the flux light curve in the 6−508 days time interval.

We obtained a final decay slope of 1.48 ± 0.03. We checked the effect on the average decay slope of our time-dependent flux conversion by applying the same procedure (steps 1, 2, and 3 above) to an unabsorbed flux light curve obtained with a uniform conversion factor and to the flux light curve in the on-line repository as well. We obtained values for the average decay slope in the 6−508 days time interval of 1.47 ± 0.02 and 1.45 ± 0.05, respectively. Both values are consistent within the errors with 1.48 ± 0.03. This suggests that our time-dependent conversion to unabsorbed flux does not affect the average decay slope of the light curve, though enhancing dispersion. Moreover, our light curve allows for a more accurate estimate of the average decay slope compared to the repository light curve.

The average decay slope value we obtained is definitely not consistent with the expected slope of $5/3$. The latter is considered a signature of tidal disruption because in the classical model by Rees (1988) and its updated versions (e.g., Lodato et al. 2009) the decay law of the mass accretion rate resulting from fall-back of the disrupted stellar debris onto the central BH is expected to be $\propto t^{-5/3}$, or at least asymptotically converging to this. The same analysis applied to the observed flux light curve has been presented in Mangano et al. (2014). In that case we obtained a final decay slope of 1.36 ± 0.02, which is consistent at the 2σ level with $4/3$, i.e. the slope value in the decay law for the jet luminosity in case of super-Eddington slim accretion disk formation (Cannizzo & Gehrels 2009). However, the average decay slope value of the unabsorbed flux light curve is also not consistent with $4/3$. The measured slope may be consistent with the TDE phenomenon when more realistic physics of accretion disks is properly taken into account (Cannizzo et al. 2011).

Could it be that the actual TDE began much earlier than the nominal March 28 BAT trigger, and therefore the decay slope calculated from the true $t = 0$ was steeper? We have investigated the possibility suggested by Tchekhovskoy et al. (2014) that the $t = 0$ time appropriate for the average light curve decay may lie earlier than the BAT trigger time by $\Delta t_{\rm offset}$ days. For this purpose, we repeated the fits of our six smoothed light curves with the model $\log_{10}(f_{\rm X}) = q - s\,\log_{10}(t + \Delta t_{\rm offset})$ and calculated the average best-fit slopes for all integer values of $\Delta t_{\rm offset}$ from 1 to 45 days. The plot of the average slope s versus $\Delta t_{\rm offset}$ is shown in Figure 12. A slope consitent with $5/3$ at 1σ is found for $\Delta t_{\rm offset} \sim 6$ days.

The degeneracy between decay steepness s and $\Delta t_{\rm offset}$ revealed in Figure 12 can be quantitatively resolved by considering the form of the decay law, and the basic properties of the TDE decay. After a TDE occurs, there is negligible accretion from stellar fallback for $\sim t_{\rm fb}$, the fallback time for the most tightly bound debris to return to the BH and to begin to accrete. Tchekhovskoy et al. (2014) suggest that following $t_{\rm fb}$ there may elapse an additional $\Delta t_{\rm offset}$ for magnetic flux accumulation in the inner disk to build up to the point that the jet becomes active. Therefore, one expects a gap of $t_{\rm fb} + \Delta t_{\rm offset}$, after which accretion begins, followed by a power law decay $\propto \left(\frac{t}{t_{\rm fb}+\Delta t_{\rm offset}}\right)^{-s}$, where $s \simeq 1-2$, in the rate of supply of fallback gas to the central engine. However, the accretion-powered jet does not become visible until a time $t_{\rm fb} + \Delta t_{\rm offset}$ following the TDE. Thus in this

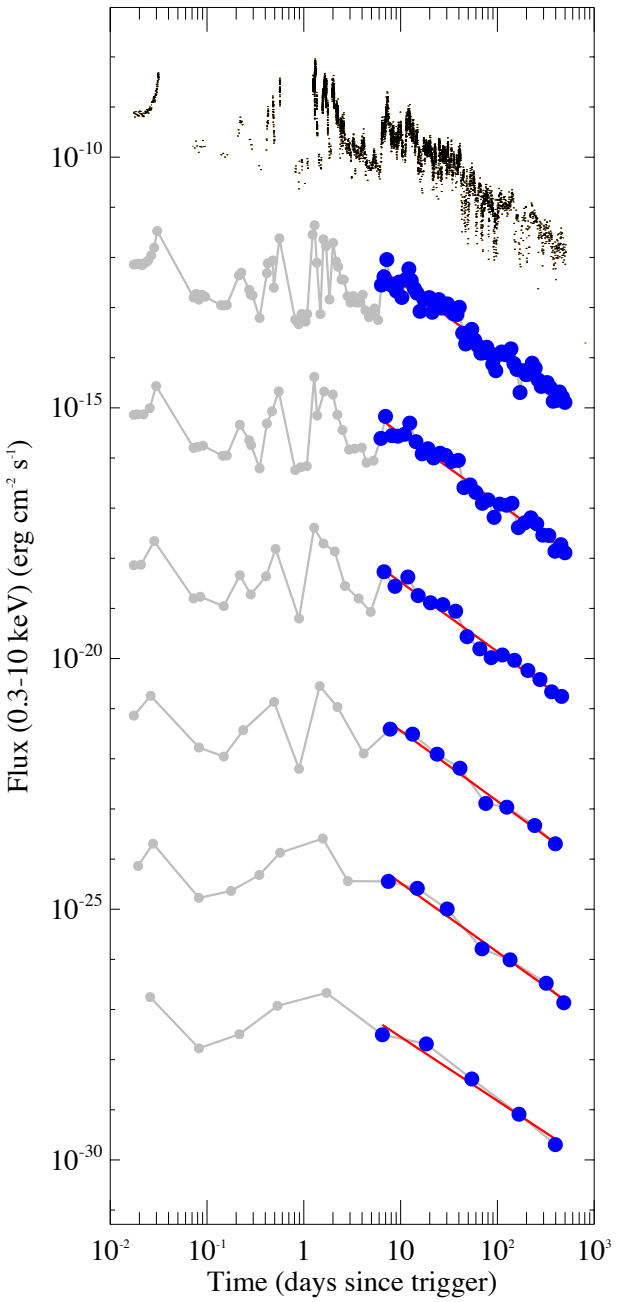

Figure 11. Results of rebinning the unabsorbed flux light curve of Swift J1644+57 using N time intervals per decade of days, equally spaced in $\log(t)$ as described in the text. From top to bottom, we plot the initial light curve and the six progressively smoothed light curves with 32, 16, 8, 4, 3, and 2 points per decade, with arbitrary normalization. Points in the time interval 6−508 days, used for the fit, are highlighted with blue markers. Solid red lines represent the linear fits in the log−log space.

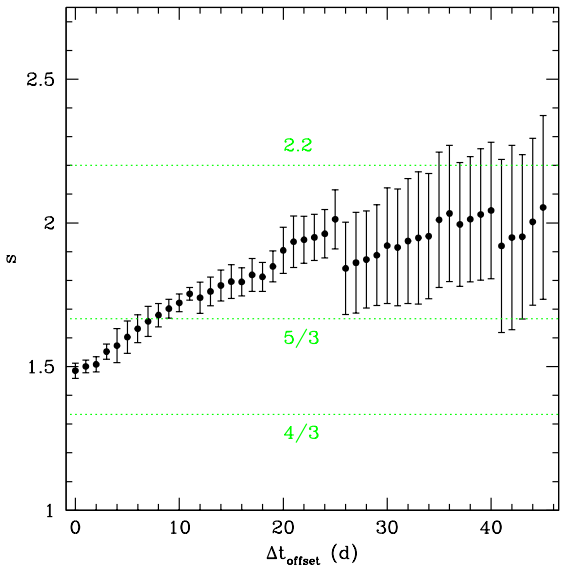

Figure 12. Average power-law decay slope of the flux light curve of Swift J1644+57 for $t > 6$ days post-trigger as a function of the offset of the tidal disruption event onset from the BAT trigger. The horizontal lines at $^4/_3$, $^5/_3$, and 2.2 represent expected values of the slope for different physical models of the disruption event.

idealization

$$f_{\rm X} = \begin{cases} 0 & t < t_{\rm fb} + \Delta t_{\rm offset} \\ f_{\rm X,max} \left(\frac{t}{t_{\rm fb}+\Delta t_{\rm offset}} \right)^{-s} & t \geq t_{\rm fb} + \Delta t_{\rm offset}. \end{cases} \quad (1)$$

Inherent in this formalism is the assumption that the jet luminosity L_J tracks the accretion rate $\dot{M}$ from the inner accretion disk onto the BH for $t \geq t_{\rm fb} + \Delta t_{\rm offset}$. The smooth power-law decay trend observed in the late XRT light curve supports the idea of a simple linear relation between L_J and $\dot{M}$ out to $t \simeq 500$ days.

By considering the ratio of the peak X-ray flux to the fluence $\Delta E_{\rm X,iso} = \int_{t_1}^{\infty} f_{\rm X}(t)dt$ where $t_1 = t_{\rm fb} + \Delta t_{\rm offset}$, one can directly measure $t_{\rm fb} + \Delta t_{\rm offset}$ (Gao 2012) . From the functional form for $f_{\rm X}(t)$, one may write

$$t_{\rm fb} + \Delta t_{\rm offset} = (s-1)\frac{\Delta E_{\rm X,iso}}{f_{\rm X,max}} \quad (2)$$

Note that since this argument depends only on the ratio of fluence and peak flux, all uncertainties such as beaming angle, accretion efficiency, jet efficiency, and distance cancel out. Using our measured values $f_{\rm X,max} \simeq 9 \times 10^{-9}$ erg cm^{-2} s^{-1} and fluence $\Delta E_{\rm X} \simeq 6 \times 10^{-4}$ erg cm^{-2} yields $t_{\rm fb} + \Delta t_{\rm offset} \simeq 0.9$ days for $s = ^5/_3$, or $t_{\rm fb} + \Delta t_{\rm offset} \simeq 0.5$ days for $s = ^4/_3$. These small values of $t_{\rm fb} + \Delta t_{\rm offset} \lesssim 1$ days argue against the possibility for $\Delta t_{\rm offset} \gtrsim 10$ days presented in Tchekhovskoy et al. (2014). For this estimate we have idealized the entire light curve with one decay law. One could in theory fit a broken power law and obtain a more precise estimate, but given that $f_{\rm X,max}$ is set by a flare during the first few days, only a rough estimate seems warranted.

5. LIGHT CURVE DIPS

Clues about the physical nature of Swift J1644+57 may come from the difference in the spectral distribution of the radiation emitted by the source during the dips and outside them. Since dips are short and often drop more than an order of magnitude from the average emission level, we cannot obtain sufficient counts for detailed spectral analysis of individual dips. Instead, we must extract a single cumulative spectrum from many dips at a time. On the other hand, we cannot merge data from different operation modes. Therefore, we consider the following two different periods during which significantly deep dips are visible in the light curve of Swift J1644+57: *(a)* from T_0+14.5 days to T_0+39.5, with XRT steadily observing in WT mode and *(b)* from T_0+40.5 days to T_0+404.8 with XRT steadily observing in PC mode.

To select the dip good time intervals (GTIs), we developed a three step procedure that can be described as follows: *(i)* fit the light curve in a given time interval to a model and calculate the weighted residuals; *(ii)* remove all points with weighted residuals lower than a fixed negative threshold, then repeat the fit until no further points need to be removed; *(iii)* shift the best-fit model down by a proper amount and save as GTIs of the dips all the time intervals including only points below the shifted model. We developed this procedure in the `IDL` programming language and making use of the fit routines in the `MPFIT` package by Markwardt (2009).

Step *(ii)* in our procedure gives us an alternative way to estimate the continuum underlying the light curve, though because of the large dispersion of the data the reduced χ^2 of the fit is not expected to assume statistically acceptable values, and the uncertainties of the model parameters are expected to be substantially underestimated. The dips represent the points with the largest deviation from the continuum and they dominate the residuals: best-fit solutions obtained without removing any point have normalizations that make them lie significantly below the bulk of the data set. The iterative removal of points with negative residuals allows us to obtain solutions that actually pass through the most densely populated region of the curve. A threshold of -5 for the weighted residuals has been chosen in order to obtain a good description of the flux light curve after 6 days, using a power-law model $f_{\rm X}(t) = Nt^{-s}$ with decay slope s fixed to the value of 1.48 estimated in Section 4. In Figure 13, the model just described is represented by the black solid line in the upper panel, and the weighted residuals in the lower panel refer to it. They suggest that the true underlying continuum is reasonably well reproduced. An equivalent description of the continuum is provided by the dashed blue line in the upper panel, representing a best-fit solution obtained with a power-law model with initial time shifted by $\Delta t_{\rm offset}$ days before the BAT trigger ($f_{\rm X}(t) = N\,(t + \Delta t_{\rm offset})^{-s}$) and slope s fixed. However, the very same relation between s and $\Delta t_{\rm offset}$ already shown in Figure 12 affects results obtained with this model. From these analyses we infer that -5 is a reasonable value for the threshold of rejection of points with negative residuals.

We applied our procedure to the count rate light curve of Swift J1644+57 computed in Section 3, separately for periods *(a)* (WT mode) and *(b)* (PC mode). We used a power-law model to fit the underlying continuum, and a threshold of -5 in step *(ii)*. We obtained

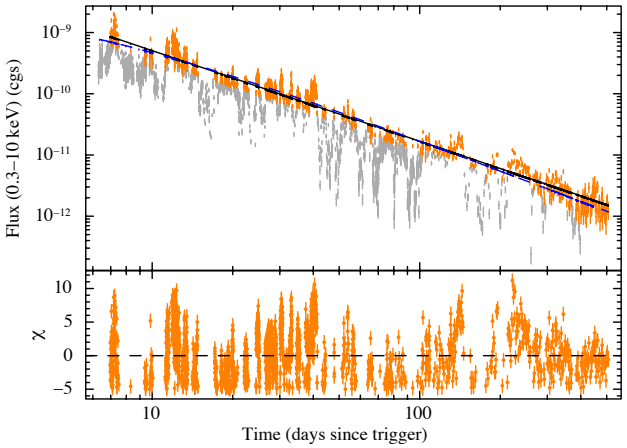

Figure 13. Fit to the X-ray flux light curve of Swift J1644+57 over the time interval from T_0+6.3 days to T_0+507 days performed with the iterative data rejection method described in the text. The black solid line in the upper panel represents the best-fit solution obtained by fitting a power law model with free normalization and slope fixed to 1.48 (expected value from estimates in Section 4). All points with weighted residuals < -5 have been removed from the fit at each successive iteration. The final sets of rejected points (1833 out of 3740) are shown in the upper panel only, in light gray. The dashed blue line in the upper panel is the best-fit solution obtained with a power-law model with initial time shifted by $\Delta t_{\rm offset}$ and slope fixed to 5/3. The value of $\Delta t_{\rm offset}$ derived after rejecting 1894 points with weighted residuals < -5 for this model is 5 days, in agreement with the plot in Figure 12.

Table 3
Swift J1644+57: GTI of the Dips

Number	t1[a] (days)	t2[b] (days)	XRT Mode
1	14.87580058	15.28213427	WT
2	15.28650302	15.29033219	WT
3	15.34551102	15.34946728	WT
35	41.84660666	42.70801067	PC
36	42.78064206	43.23784472	PC
37	43.70705003	43.82982205	PC

Note. — This table is published in its entirety in the electronic edition of the Astrophysical Journal. A portion is shown here for guidance regarding its form and content.

[a]Starting time of data interval, relative to the first BAT trigger at T_0 = 2011 March 28 12:57:45.201 UTC = 55648.5401 MJD.
[b]Ending time of data interval, relative to the first BAT trigger at T_0 = 2011 March 28 12:57:45.201 UTC = 55648.5401 MJD.

power-law decays with slopes 0.83 ± 0.08[8] for period *(a)* and 1.390 ± 0.005 for period *(b)*, respectively. Finally, we shifted each power-law model down by decreasing its normalization by a quantity equal to 5 times the average percentage error of the light curve points in the corresponding period, and defined the GTIs of the dips in each period as in step *(iii)*. We merged together successive time intervals containing only points below the cutting line whenever they were not separated by at least one point at a rate 10% larger than the cutting line. The final time selection, consisting of 98 GTIs (34 in WT mode and 64 in PC mode), is listed in Table 3. Figure 14 shows the separation between the "normal" and "dip" time intervals for the WT and PC mode data. Figure 15 shows a composite normalized light curve obtained by dividing each segment of the rate light curve by the corresponding cutting line. In this representation, the dips are the points below 1, and the depth of each dip is measured by the normalized rate level of its minimum, the inverse of which tells us by what factor the point is below the cutting line. In Figure 15 the dips' minima are marked with an empty star if the corresponding GTI is longer than 0.5 days, or with an empty circle if it is shorter. Note that the durations of our GTIs span from ∼190 s to ∼16.5 days, with 41 of them longer than 0.5 days and 57 shorter. Moreover, the short GTIs are all concentrated in the first 90 days and are not deeper than 0.2, with an average depth of ∼0.8, while the long GTIs are uniformly distributed, with depths in the range 0.87−0.08 and average depth ∼0.36. It is likely that the absence of short GTIs after 90 days is a side-effect of the differential binning of the light curve, requiring longer time bins at later times, and average bin duration larger than 0.1 days after the first 100 days. If we define the dynamic range of a dip to be the ratio between the maximum count rate since the end of the preceding dip and the minimum count rate of the dip in question, we see that the short dips have a small dynamic range (between 1.1 and 6.3 with an average of 2.3), while the long dips have a much larger dynamic range (between 2 and 54 with an average of 10).

[8] Errors on best-fit parameters given by `MPFIT` are at 1σ confidence, but in this case they are likely underestimated by at least an order of magnitude.

With the GTIs of the dips in Table 3 we have been able to extract cumulative "dip" and "normal" spectra for each observing period, and corresponding backgrounds. We fit the resulting four spectra with both an absorbed power-law and an absorbed log-parabola spectral model, and selected the best-fit model via an F-test as already done with time resolved spectra in Section 3.3. The final best-fit parameter values are listed in Table 4, with corresponding confidence contours plotted in Figure 16. The final spectral fits are shown in Figure 17. In both periods, the "dip" and "normal" spectra have the same shape (absorbed log-parabola for WT spectra in period *(a)*, and absorbed power-law for PC spectra in period *(b)*) and the same level of absorption (i.e. consistent values of N_H). The values of the photon indices though indicate that "dip" spectra are generally softer. This is in agreement with the harder-when-brighter correlation on short timescales described in Section 3.3. Moreover, there is evidence for larger intrinsic N_H in PC (i.e. at later times) than in WT (only marginal for "dip" spectra), in agreement with the trends observed in the top panel of Figure 5 and in the right panel of Figure 7.

6. DISCUSSION

We have calculated the definitive X-ray light curve of Swift J1644+57 in the 0.3−10 keV band as observed by *Swift*/XRT in three years of follow-up and monitoring since the detection of the outburst.

The overall shape of the light curve consists of a set of initial spiky flares followed by an episode of steep decay underlying variability on shorter time scales from about 2 to 6 days after the BAT trigger (see Figure 9, bottom panel), then a fast rebrightening by about an order of magnitude, and finally a long fading phase with a power-

Table 4
Swift J1644+57: Spectral Analysis in and Outside Dips.

Type	XRT Mode	Exposure (ks)	N_H (cgs)[a]	Photon Index[b]	β	χ^2	dof	Flux (cgs)[c]
normal	WT	177.705	$1.42^{+0.05}_{-0.05}$	$1.37^{+0.08}_{-0.08}$	$-0.36^{+0.07}_{-0.07}$	942.714	791	$71.75^{+0.48}_{-0.56}$
dips	WT	117.681	$1.43^{+0.11}_{-0.11}$	$1.50^{+0.17}_{-0.17}$	$-0.32^{+0.15}_{-0.15}$	641.985	627	$26.77^{+0.34}_{-0.46}$
normal	PC	1074.540	$1.84^{+0.04}_{-0.04}$	$1.51^{+0.02}_{-0.02}$	–	802.450	743	$7.18^{+0.06}_{-0.06}$
dips	PC	325.291	$1.78^{+0.10}_{-0.10}$	$1.69^{+0.05}_{-0.05}$	–	359.828	383	$2.80^{+0.06}_{-0.07}$

[a]Units are 10^{22} cm^{-2}.
[b]Gives the value of the parameter α of the log-parabola model when the value of β is listed.
[c]Observed flux in the 0.3−10 keV band in units of 10^{-12} erg cm^{-2} s^{-1}.

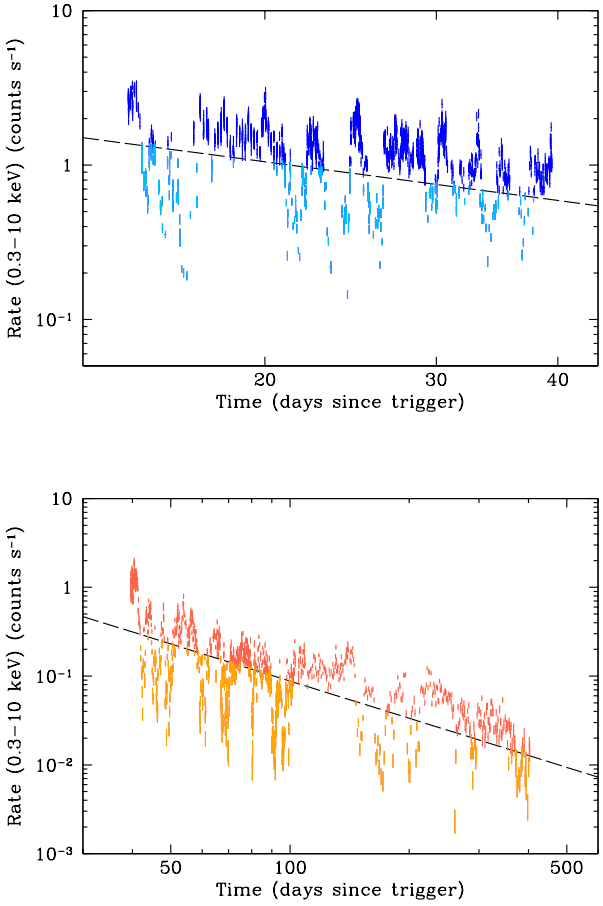

Figure 14. X-ray light curves showing the regions we identify as dips. **Top panel:** dips found during the observation period from T_0+14.5 days to T_0+39.5 days (period *(a)* in the text) in WT mode. **Bottom panel:** dips found from T_0+40.5 days to T_0+404.8 days (period *(b)* in the text) in PC mode. In both panels, the dashed line represents the cut between "normal" (above the line) and "dip" (below the line) time intervals, obtained as described in the text.

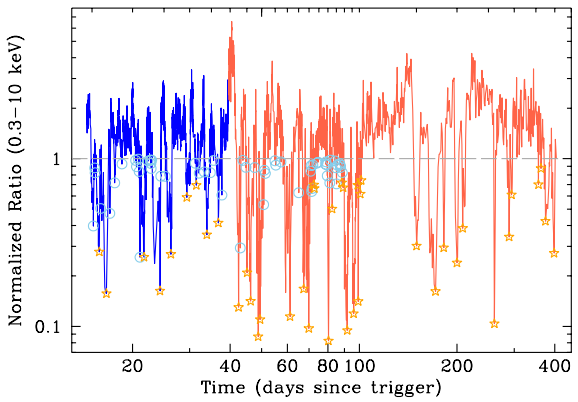

Figure 15. Composite light curve obtained dividing the light curves in Figure 14 by their cutting lines. Blue data (before T_0+39.5 days) are in WT mode and red data (after T_0+39.5 days) are in PC mode. The horizontal grey dashed line at level 1 is the new global cutting line defining the dips. Orange stars indicate the minima of the long (>0.5 days) dips and light blue empty circles the minima of the short dips.

law like average decay abruptly ending on 2012 August 17, 507 days after the trigger. Without this sudden shut-off the source would have remained fairly bright for about 8−10 years.

Despite several claims in the literature that the X-ray decay follows a $t^{-5/3}$ power law (e.g., Metzger et al. 2012; Lei et al. 2013; Kawashima et al. 2013; Kumar et al. 2013; Barniol Duran & Piran 2013; Zauderer et al. 2013; Shen & Matzner 2014; Tchekhovskoy et al. 2014), we find that this is not the case. Our modeling of the flux light curve from 6.3 to 507 days after the trigger (performed in Section 4) gives us an estimate of the decay slope of 1.48 ± 0.03 and shows that the data may be almost equivalently described with a slightly steeper slope when the decay start time is earlier than the BAT trigger by $\Delta t_{\rm offset}$ days, provided that $\Delta t_{\rm offset}$ is not larger than a few.

6.1. *Model Interpretation*

Zauderer et al. (2013) argue that the rapid decline of the X-ray flux at $t \simeq 500$ days heralded the turning off of the relativistic jet in Swift J1644+57. They suggest that at that time, the accretion rate within the jet feeding the BH dropped below the Eddington rate, $\dot{M}_{\rm Edd} \simeq 6 \times 10^{-3}$ M$_\odot$ yr^{-1}, assuming $M_{\rm BH} \simeq 10^{6.5}$ M$_\odot$ and a conversion efficiency between rest-mass energy and accretion luminosity of $\epsilon_{\rm acc} \simeq 1$. Prior to this time, the ratio of accretion power to jet power was constant, as evidenced by the constancy of the observed power law decay index. During the time it was seen by XRT, the X-ray luminosity of Swift J1644+57 varied over a dynamic range

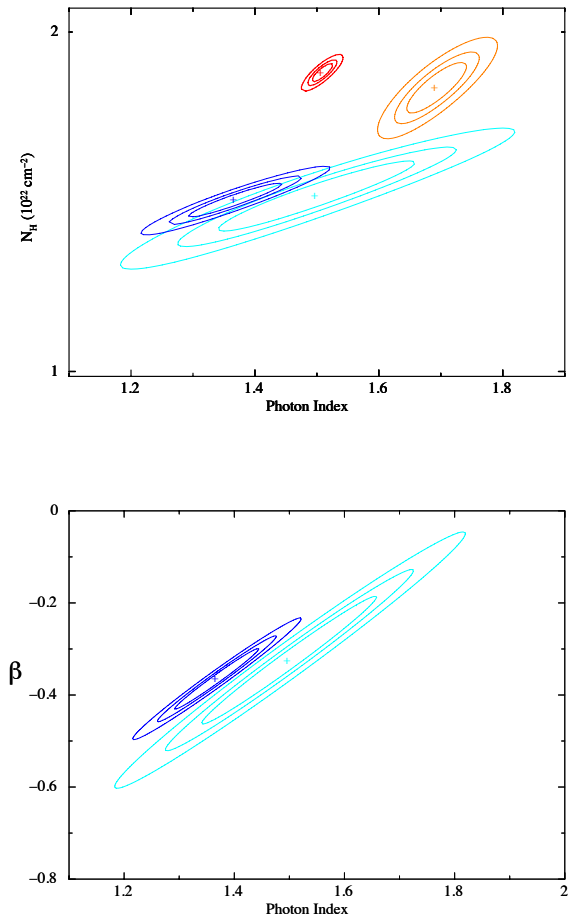

Figure 16. **Top panel:** contours at the 68%, 90%, and 99% confidence level for N_H versus photon index, obtained from the fits of "normal" and "dip" spectra in WT and PC mode (see results in Table 4, color coding is as in Figure 17). **Bottom panel:** as in the top panel, for β versus photon index.

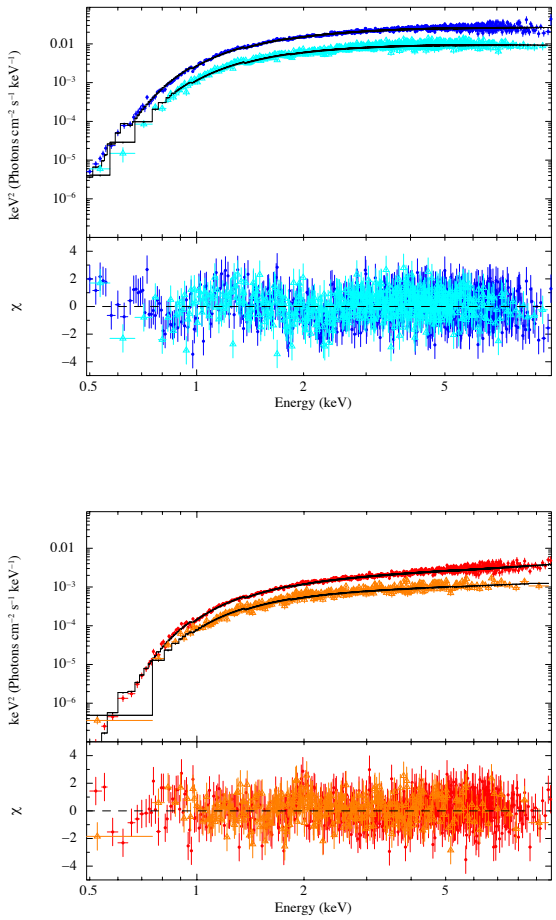

Figure 17. X-ray spectra obtained during the "normal"decay, compared with the cumulative spectra of the dips. **Top panel:** WT mode observation from T_0+14.5 days to T_0+39.5 days: "normal" spectra in blue circles and "dip" spectra in cyan triangles. **Bottom panel:** PC mode observation from T_0+40.5 days to T_0+404.8 days: "normal" spectra in red circles and "dip" spectra in orange triangles. The corresponding spectra are clearly similar in shape, i.e. fit by the same model. See fit results in (see Table 4).

of about a factor of ∼6000, from $\sim 2.2 \times 10^{48}$ erg s^{-1} to $\sim 3.7 \times 10^{44}$ erg s^{-1}. Thus if the switch-off luminosity corresponded to Eddington, at peak luminosity the accretion rate onto the BH would have been ∼6000 times Eddington.

If the conjecture by Zauderer et al. (2013) is correct, one may obtain a constraint on the combination of efficiency parameters relating accretion rate to jet power. The jet power can be expressed as

$$L_J = \epsilon_J \dot{M}_{\rm fb} c^2, \quad (3)$$

and the observed X-ray luminosity (assuming all the jet power is in X-rays) is

$$L_{\rm X,iso} = \frac{L_J}{\frac{1}{2}{\theta_J}^2}, \quad (4)$$

where θ_J is the jet opening angle. Hence,

$$L_{\rm X,iso} = \frac{\epsilon_J \dot{M}_{\rm fb} c^2}{\frac{1}{2}{\theta_J}^2}. \quad (5)$$

Assuming that the jet turns off when the accretion rate drops below Eddington, which happens at $\dot{M}_{\rm fb} = 6 \times 10^{-3}$ M$_\odot$ yr^{-1} and $L_{\rm X,iso} = 3.7 \times 10^{44}$ erg s^{-1}, we obtain the constraint

$$\epsilon_J {\theta_J}^{-2} = 5.4. \quad (6)$$

According to theory, it is not expected a priori for jet power to track accretion rate in the disk. If the jet is fed via the canonical Penrose-Blandford-Znajek process, the jet power would be

$$L_J = 1.2 \times 10^{46} \text{ erg s}^{-1} \Phi^2_{*,30} M^{-2}_{\rm BH,6} {\omega_H}^2 f(\omega_H), \quad (7)$$

where $\Phi_{*,30}$ is the magnetic flux threading the BH event horizon in units of 10^{30} Gauss cm^2, $M_{\rm BH,6}$ is the BH mass in units of 10^6 M$_\odot$, $\omega_H = a/(1+\sqrt{1-a^2})$ is the dimensionless angular frequency of the BH horizon, and $f(\omega) = 1 + 0.35{\omega_H}^2 - 0.58{\omega_H}^4$ is a high spin correction (Tchekhovskoy et al. 2010, 2014). For a spin parameter $a = 0.9$ this becomes

$$L_J = 5 \times 10^{44} \text{ erg s}^{-1} \Phi^2_{*,30} M^{-2}_{\rm BH,6}. \quad (8)$$

Tchekhovskoy et al. (2014) argue that in order for the jet power to track the accretion rate, there must exist a "magnetically-arrested" accretion disk (MAD), in which the magnetic flux threading the BH is determined by the ram pressure of the accretion flow. For such disks $\epsilon_J \simeq 1.3a^2$, where a is the dimensionless spin of the BH. For a nominal jet opening angle $\theta_J \simeq 0.1$, our constraint $\epsilon_J {\theta_J}^{-2} = 5.4$ implies a spin $a \simeq 0.2$ if Tchekhovskoy et al. (2014) are correct. Also, the MAD state may be consistent with super-Eddington accretion.

At some point during the fallback of debris from the TDE an accretion disk is expected to form and to dominate the decay law, due to its slower inherent time scale enforced by an ever-expanding outer edge to the accretion disk (Cannizzo et al. 1990, 2011). Cannizzo et al. (2011) argued that for Swift J1644+57 this transition occurred at $t \simeq 10$ days, such that for $t > 10$ days the decay law would be flatter, $s \simeq 4/3$. In this work we show that the best fit to the decay of Swift J1644+57 appears to be in line with $s = 1.5$. Moreover, the quality of the fit is good; therefore $s = 5/3$ appears to be excluded, as does the value $s = 4/3$ expected from an advective disk. As a caveat on drawing any strong conclusions based on our putative slope $s = 1.5$ for the unabsorbed flux light curve, we note that we are averaging over large amplitude variations in flux versus time. Although we utilize a multi-time step technique and average values in $\log F_x - \log t$ space, it may be that our measured s value is not robust enough to warrant a detailed comparison with either of the two canonical theoretical s values. Our small inferred value for the fallback time $t_{\rm fb} \lesssim 1$ day appears to rule out the large $\Delta t_{\rm offset}$ values that would be required to substantially increase s. The theoretical decay law $s = 4/3$ (Kumar et al. 2008; Metzger et al. 2008, 2009; Cannizzo & Gehrels 2009) is dependent on a super-Eddington disk and differs from the $s = 19/16$ expected from a standard thin disk (Cannizzo et al. 1990). This flatter decay ($s \simeq 1.19$) can also be strongly excluded from our fit, and would not be expected anyway since $\dot{M} \gg \dot{M}_{\rm Edd}$ for Swift J1644+57.

Two schools of thought have emerged concerning the fallback time $t_{\rm fb}$ for Swift J1644+57. Cannizzo et al. (2011) and Gao (2012) argue for $t_{\rm fb} \lesssim 1$ day, which leads to the inference of a tidal disruption radius to periastron radius ratio $R_T/R_P \simeq 10$ for the TDE, whereas Tchekhovskoy et al. (2014) and Shen & Matzner (2014) find $R_T/R_P \simeq 1$. Shen & Matzner (2014) also favor a BH mass $M_{\rm BH} \simeq 10^4 - 10^5$ M$_\odot$, lower than most other groups. They advocate $t_{\rm fb} \gtrsim 10$ days and assume that the $s = 5/3$ decay starts at $\sim$10 days, which is not consistent with our results. It is also important to note that Tchekhovskoy et al. (2014) and Shen & Matzner (2014) simply use the Swift J1644+57 data taken from the XRT website (Evans et al. 2009) which assumes a single ECF (4.8×10^{-11} erg cm^{-1} count^{-1}) and reports the *observed* flux, whereas we have used the time-dependent ECF for the unabsorbed flux, which is related to the intrinsic luminosity. As we show in Figure 6, the unabsorbed flux ECF is about 9.6×10^{-11} erg cm^{-1} count^{-1}, resulting in fluxes a factor of 2 higher than those obtained with the standard analysis; this affects the energetics, but not the derived decay slope s of the light curve.

An important caveat to the results of Cannizzo et al. (2011) and Gao (2012) has emerged in the past few years, namely, these studies adopted a theoretical value for $t_{\rm fb}$ from Lacy et al. (1982) and Rees (1988) that derives from relating the spread in specific orbital energy of the debris streams to conditions at periastron, $\Delta\epsilon \simeq GM_{\rm BH}R_*{R_P}^{-2}$. However, recent work has shown that this viewpoint is not correct: the stellar shredding by the tidal force is in fact so effective that by the time the star arrives at periastron, its shredded fragments are traveling on ballistic trajectories; therefore the relevant radius in determining $\Delta\epsilon$ and thus $t_{\rm fb}$ is not the periastron radius R_P, but rather the disruption radius R_T (Guillochon & Ramirez-Ruiz 2013; Stone et al. 2013). This leads to smaller $\Delta\epsilon$ and larger $t_{\rm fb}$. However, the more recent studies do not consider strong general relativistic effects under the Kerr metric, which would become relevant if an orbit were deeply plunging such that R_P were to lie within the ergosphere of a nearly maximal spin BH. It is conceivable $t_{\rm fb}$ could be shortened dramatically. Support for this idea may be given by a recent study by Evans et al. (2015) which presents a new class of TDEs showing prompt formation of an accretion torus and hyperaccretion. These TDEs involve ultra-close encounters ($R_T/R_P \simeq 10$) and high spin BHs. They find a strong influence of general relativistic effects. A caveat to their work is that their large $\Delta\epsilon$ values may be an artifact of under-resolving the midplane compression of the star.

In any event, the observational inference on the fallback time we derive in this work, $t_{\rm fb} \lesssim 1$ days, is based on two observables, the peak X-ray flux and the total X-ray fluence, and is therefore not subject to the theoretical uncertainties inherent in the aforementioned works. Krimm & Barthelmy (2011) note apparent activity in Swift J1644+57 on 2011 March 25, $\sim$ 3 days before the 2011 March 28 *Swift*/BAT trigger. This interval of time exceeds our nominal $t_{\rm fb}$ estimate. The signal-to-noise (S/N for the 2011 March 25 was low, $\sim 3.7\sigma$ (0.0059 ± 0.0016 ct s^{-1} cm^{-2}), but the positional coincidence with the larger trigger three days later, S/N= 7.6σ, gives strength to the detection. A prior close encounter of the star that became disrupted may have led to a partial disruption, such that an extended train of debris arrived near the BH prior to the main TDE, leading to a weak precursor.

6.2. *Residual X-ray Emission and Future Evolution*

Swift J1644+57 is still detected at the flux level of $(1.0\pm 0.8)\times10^{-14}$ erg cm^{-2} s^{-1} (0.3−10 keV, observed flux) over an integrated exposure of $\sim$200 ks accumulated in $\sim$500 days of weekly XRT monitoring. The *Chandra*-ACIS ToO observation performed on 2012 November 26, $\sim$3 months after the XRT drop, also detected Swift J1644+57 with 2.8σ significance. A detailed analysis of the observation is reported in Zauderer et al. (2013). We reproduced their results and estimated a 0.3−10 keV unabsorbed flux[9] of $(7\pm3)\times10^{-15}$ erg cm^{-2} s^{-1}, consistent with the final *Swift*/XRT data point (see Figure 9). This flux value is obtained with the average late XRT spectral parameters estimated and used by (Zauderer et al. 2013): $N_{\rm Hgal}$ fixed to 1.7×10^{20} cm^{-2}, intrin-

[9] Flux error for *Chandra* points is at the 68% confidence level.

sic $N_H \sim 1.4 \times 10^{22}$ cm^{-2}, and $\Gamma \sim 1.3$. A fit with N_H fixed to 1.9×10^{22} cm^{-2} gives $\Gamma = 2.1^{+1.7}_{-1.4}$ (consistent with the spectrum of our XRT last point presented in Section 3.3) and an unabsorbed 0.3−10 keV flux of $(8\pm3)\times10^{-15}$ erg cm^{-2} s^{-1}. In the second observation performed by *Chandra* on 2015 February 17 (day 1421 after the BAT trigger), Swift J1644+57 is still detected with 5σ significance and net count rate of $(4.2\pm1.2)\times10^{-4}$ counts s^{-1} in the 0.5−8 keV range. We modeled the spectrum with an absorbed power-law model as we already did with previous data. Fixing N_{Hgal} to 1.7 $\times10^{20}$ cm^{-2}, and intrinsic N_H to $\sim 1.4\times10^{22}$ cm^{-2} we obtain $\Gamma = 0.6 \pm 1.2$, $\chi^2_r = 0.906$ (10 dof), while N_H fixed to 1.9×10^{22} cm^{-2} gives $\Gamma = 0.74 \pm 1.2$, $\chi^2_r = 0.932$ (10 dof). The unabsorbed flux in the (0.3−10) keV band is equal to $(1.7^{+0.4}_{-1.0})\times10^{-14}$ erg cm^{-2} s^{-1}. The 2015 *Chandra* spectrum seems to be harder than both the *Swift*-post drop spectrum and the *Chandra* 2012 spectrum, though given the large uncertainties on the photon indices the statistical significance is marginal. Moreover, this 2015 detection is still consistent with the final *Swift*/XRT data point (see Figure 9).

The residual emission detected by *Chandra* and *Swift* is not consistent with thermal emission from the fall-back accretion disk. For M_{BH} in the $5\times10^6-10^7$ $M_\odot$range, the disk is expected to have a temperature at the inner radius in the ∼20−25 eV range if jet shut-off occurred at a critical accretion rate $\sim\dot{M}_{Edd}$, or in the ∼12−15 eV range if the critical accretion rate was ~0.1 $\dot{M}_{Edd}$. By using the `diskbb` model in `xspec` with true inner radius ~6 G M_{BH}/c^2, face-on disk, and redshift effects properly taken in account, we predict a 0.3−10 keV flux always $< 10^{-16}$ erg cm^{-2} s^{-1}, and a bolometric disk luminosity L_{disk} in the $5\times10^{43}-10^{45}$ erg s^{-1} range. By using the standard spectral model for Comptonized X-ray emission from an AGN corona described in Ghisellini & Tavecchio (2009), which consists of a power-law with photon index ~ -1, a high energy exponential cut-off with folding energy of ∼150 keV, and total X-ray luminosity ~0.3 L_{disk}, we can easily calculate that the observed 0.3−10 keV flux could be obtained as a result of Comptonization of the disk UV photons by a hot corona for an $L_{disk} \lesssim 10^{44}$ erg s^{-1}. However, fine tuning of a number of unmeasurable parameters is required to achieve this result, and this makes the interpretation of residual X-ray emission from Swift J1644+57 as Comptonized emission unlikely, though we cannot rule out contributions from Comptonization effects.

An alternate interpretation is that the residual X-ray emission detected by *Chandra* and *Swift* after jet shut-off originates from the forward shock of the jet still expanding in the ambient medium. In fact, Zauderer et al. (2013) calculate that the low X-ray flux measured by *Chandra* is consistent with synchrotron emission from the forward shock of a structured jet with time-dependent physical parameters derived by modeling the radio spectra of Swift J1644+57, which they regularly monitored for about 600 days after the outburst. In this scenario we expect the X-ray emission to go on decaying with time as the radio emission. An extrapolation of the 2012 *Chandra*-ACIS flux to 2015 can be done assuming no spectral variation with time (as guaranteed by the extrapolated value of the cooling frequency based on Zauderer et al. (2013) results still being in the NIR band), and a flux decay rate $\propto t^{-\alpha}$ with $\alpha \sim (2-3p)/4$, where p is the slope of the energy distribution of the electrons accelerated at the shock (Granot & Sari 2002). For a typical value of $p \sim 2.2-2.6$, we expect α in the 1.15−1.45 range. Then, an unabsorbed flux lower than $\sim (2.6\pm1)\times10^{-15}$ erg cm^{-2} s^{-1} in the 0.3 – 10 keV band was expected in February 2015. The 2015 *Chandra* detection clearly shows that the X-ray flux has not decayed according to this prediction. Unfortunately, we have no simultaneous information on radio emission level from Swift J1644+57 and we cannot tell if the two bands are really evolving in an independent way. Only a coordinated X-ray and radio monitoring will be able to answer this question.

A distinctive signature of the two possible scenarios for the origin of residual X-ray emission, i.e. disk/corona related Comptonized emission and forward shock related synchrotron emission, may be the photon index of the X-ray spectrum Γ. In the former case, Γ is expected to lie in the $1.5-2.2$ range: values much lower than 1.5 correspond to nonphysical Compton y parameters in standard inverse-Compton scattering scenarios for modeling the X-ray power-law emission from the corona (Zdziarski et al. 1990); values much larger than 2.2 are observationally unlikely based on detailed X-ray spectral analysis of the non-beamed AGNs (Corral et al. 2011; Vasudevan et al. 2013). In the latter case, since the Zauderer et al. (2013) analysis shows that the cooling frequency of the shocked electrons was and is likely still expected to be in the infrared band, the spectral slope in X-rays should be $\Gamma = p/2 + 1$, and for a typical value of $p \sim 2.2 - 2.6$, we expect $\Gamma \sim 2.1 - 2.3$ (Granot & Sari 2002). Unfortunately, none of our *Swift* or *Chandra* X-ray spectra has enough statistics to unambiguously constrain the photon index. Even our indication in favor of a $\Gamma > 2$ given by the measure of the XRT band ratio after the shut-off (see Section 3.2) does not allow us to decide between the two cases.

Krolik & Piran (2011) and Bloom et al. (2011) point out that the variability time-scales observed in Swift J1644+57 are orders of magnitude shorter than those found in the relativistic jets of blazars, which presumably have a similar mechanism (Blandford-Znajek Blandford & Znajek 1977). Tchekhovskoy et al. (2014) provide a model that seems able to account for all of the behavior seen in the X-ray light curve of Swift J1644+57, including both the initial rapid and strong variability in 2011 March as well as the sudden shut-off in 2012 August. The uncertainty regarding the long term evolution of the whole system after jet shut-off, the nature and timescales of possible future disk transitions and their observable signatures are related to the uncertainty in the physics of disk accretion and to the detailed accretion disk models adopted by different authors. According to Tchekhovskoy et al. (2014) a reactivation of the jet may occur due to a further transition of the disk to the Advection Dominated Accretion Flow (ADAF) stage expected for $\dot{M} \lesssim 0.01$ $\dot{M}_{Edd}$. This phenomenon is expected in analogy to state transitions from high/soft to low/hard emission observed in Galactic microquasars, and observationally associated with a jet revival (Fender et al. 2004). The jet reactivation, predicted to occur some-

time between 2016 and 2022 at an X-ray flux level of $\sim 10^{-14} - 10^{-13}$ erg cm^{-2} s^{-1} (depending on M_{BH} and the type and the disrupted fraction of the passing star), is expected to be observable for months. The new X-ray bright stage of Swift J1644+57 will likely be detectable by *Chandra* through all the reactivation period, and possibly even by *Swift*. In the final analysis, such questions will be decided by observations, and to this end *Swift* continues to observe Swift J1644+57 regularly, watching for another flare-up of this fascinating object.

6.3. *Spectral Analysis and Dips*

We have shown that the shape and the variability timescales in the X-ray light curve of Swift J1644+57 are unlike other known sources with relativistic jets along the line of sight. The spectral behavior of Swift J1644+57 is peculiar as well. For the first several days the source seems to follow a pure harder-when-brighter correlation similar to that observed in blazars, but the later time analysis we have done can be better explained in terms of a superposition of a slow hardening of the spectra along with the global light curve decay, and a harder-when-brighter correlation tracking variability at shorter timescales. The typical harder-when-brighter behavior in blazar flares can be explained in terms of the blazar spectral model (Celotti & Ghisellini 2008) by a rise of the External Compton (EC) component with the accretion rate, associated with an independent different evolution of the Synchrotron Self Compton (SSC) component. It has also been observed that the slope of the correlation between the photon index and the 2−10 keV flux can be different from flare to flare, and can even disappear (Vercellone et al. 2011). This may happen when the SCC and EC components increase proportionally with the accretion rate but maintain balance, so that luminosity rises achromatically.

Paper I successfully explained the early broadband spectra of Swift J1644+57 with a blazar-like spectral model, but no EC component was required by our data. The stringent VERITAS and *Fermi* upper limits on gamma-ray emission even required a suppression of the Self Compton peak of the spectrum through pair production. The EC component in blazars can be produced by seed photons from the Broad Line Region (BLR) and/or seed photons from the accretion disk interacting with the relativistic electrons in the jet. Actually, it is very unlikely that a BLR had time enough to form in the case of Swift J1644+57, but it is still possible that EC from disk photons contributes to the soft X-ray emission of Swift J1644+57, though the component peak, expected at very high energies, must be highly suppressed. On the other hand, Paper I (e.g. Supplementary Figure 15) showed that both the XRT spectrum extracted at the light curve minimum 4.5 days post-trigger and the later intermediate level spectrum extracted at 8 days post-trigger have an upward kink at higher energies that suggest the presence of an unknown additional hard spectral component, the peak of which they could not constrain. This is also the case for all our XRT spectra fit by a concave log-parabola model. This unknown hard component may play a role similar to the low energy tail of the EC in determining the spectral evolution of Swift J1644+57 in X-rays.

The softness of the average emission of the dips compared to the inter-dip normal emission, without N_H variation, agrees with a production mechanism based on a larger contribution of a hard spectral component at larger accretion rate/luminosity. The apparent randomness in temporal distribution, duration, and depths of the dips, as well as in height, duration, and structure of the flares occurring between dips, suggest they originate from random fluctuations in the accretion rate, i.e. instabilities in the accretion flow, like in blazars. However, dynamic range and duty cycle of dips and flares in Swift J1644+57 are extreme compared to blazars, and are difficult to reproduce in this model. Krolik & Piran (2011) suggest that the required extremely compact and short-lived inhomogeneities (i.e. "knots") in the accretion flow, can be obtained if the tidally disrupted star is a white dwarf and the tidal disruption goes on taking away fragments of it at each periastron passage until it is consumed. However, only a central BH mass of $\sim 10^4$ $M_\odot$ would fit the observed timescales, which is not consistent with results from our analysis of the global decay of the Swift J1644+57 light curve. An alternative mechamism based on random internal shocks propagating along the jet channel has been proposed by De Colle et al. (2012). Based on a hint of possible periodic modulation of the dips, Saxton et al. (2012) proposed they may be due to combined effects of precession and nutation that cause the core of the jet briefly to go out of the line of sight.

7. CONCLUSIONS

We present the definitive *Swift*/XRT light curve for Swift J1644+57, which spans ∼800 days. We find that the ECF varies over time due to spectral evolution. Most previous studies of the long term Swift J1644+57 relied on a single ECF for the entire light curve. The peak flux, at $(t - T_0) = 1.3$ days, was $\simeq 9 \times 10^{-9}$ erg cm^{-2} s^{-1}, and the fluence over the entire light curve was $\simeq 6 \times 10^{-4}$ erg cm^{-2}. With the standard cosmology, a redshift $z = 0.354$ yields peak luminosity and total energy values of $\sim 2 \times 10^{48}$ erg s^{-1} and $\sim 2 \times 10^{53}$ erg, respectively. From the ratio of these numbers we determine an observationally based value for the fallback time for debris following the TDE of $t_{\rm fb} \lesssim 1$ days. By fitting the decay slope for 6 days $< t <$ 508 days for six logarithmic binnings in $\log \Delta t$ we determine a post-fluctuation decay slope $s = 1.48 \pm 0.03$. This is statistically distinguishable from the $s = 5/3$ value for Swift J1644+57 commonly cited in the literature, and also from the $s = 4/3$ value advocated by Cannizzo et al. (2011) and Gao (2012) wherein one has a rapid transition from stellar fallback to highly advective disk accretion. Given the large fluctuations in X-ray flux with time, it may be difficult even with our multi-time step averaging technique to reliably extract a physically meaningful slope which bears comparison to theory. Previous studies quoting a slope did not carry out detailed fitting but simply overlay a $s = 5/3$ decay onto $\log f_X - \log t$ light curve for Swift J1644+57 taken from the *Swift*/XRT website, which assumes a single ECF value.

Our small inferred $t_{\rm fb}$ supports the viewpoint of a rapid transition from stellar fallback to disk accretion (Cannizzo et al. 2011; Gao 2012) but the value of $s \approx 1.5$ does not. A value $t_{\rm fb} \lesssim 1$ day challenges current theory, which favors $t_{\rm fb} \simeq 20 - 30$ days, but does not consider strong general relativistic effects in the Kerr metric for

large R_T/R_P encounters; modifications in the binding energy spread $\Delta\epsilon$ for the tidal debris from the standard results for $R_T/R_P \simeq 1$ encounters are treated via linear perturbations to a Newtonian gravitational potential (e.g., Guillochon & Ramirez-Ruiz 2013; Stone et al. 2013, – see their Section 6).

For completeness we note that several recent works have addressed the issue of the fate of the shredded gas following the TDE (Hayasaki et al. 2013, 2015; Shiokawa et al. 2015; Bonnerot et al. 2015; Guillochon & Ramirez-Ruiz 2015). Shiokawa et al. (2015) consider the $R_T/R_P = 1$ tidal disruption of a 0.64 $M_\odot$ WD by a 500 $M_\odot$ Schwarzschild BH utilizing a general relativistic hydrodynamic simulation (excluding magnetic fields). They find deflection of mass by shocks to be an important effect. The peak accretion rate is lowered by about a factor of ten compared to previous estimates and the duration of the peak is enhanced by about a factor of five. Bonnerot et al. (2015) investigate $R_T/R_P = 1$ and $R_T/R_P = 5$ tidal disruptions of a 1 $M_\odot$ star by a 10^6 $M_\odot$ Schwarzschild BH using an SPH (smoothed particle hydrodynamics) code. They find that circulation of debris is driven by relativistic apsidal precession (which causes the leading part of the stream to collide with the trailing part that is still falling back toward the BH). They consider two cooling efficiencies, isothermal and adiabatic equations of state. Guillochon & Ramirez-Ruiz (2015) carry out simplified Monte Carlo realizations of tidal disruption streams to determine their structure prior to circularization. They find that for SMBHs with $a \gtrsim 0.2$ the stream self-intersection happens after the most bound debris has wound around periapse many times, and thus one expects the accretion rate onto the BH to be delayed with respect to the fallback rate, $\dot{M}_{\rm acc}(t + t_{\rm delay}) = \dot{M}_{\rm fb}(t)$. This delay would occur in addition to the one posited by Tchekhovskoy et al. (2014) by considering magnetic flux build-up near the BH. The results of Guillochon & Ramirez-Ruiz (2015) are particularly interesting in light of our observational result $t_{\rm fb} + \Delta t_{\rm offset} \lesssim 1$ day and indicate that additional physical effects may be required to address the unique aspects of Swift J1644+57.

We cannot favor an interpretation of the late time low-level X-ray emission by *Chandra* and *Swift* as being consistent with emission from the forward shock of a structured jet because the second *Chandra* observation performed at the beginning of 2015 shows that the X-ray flux has not decayed as expected in this scenario from an extrapolation of the radio decay trend. However, further coordinated X-ray and radio monitoring of the source is needed to rule out the suggested common origin of the residual X-rays and the radio emission. The low-level X-ray emission is not consistent with thermal emission from the fallback accretion disk expected at these late times, but maybe reconciled with a scenario including Comptonized emission from a hot corona.

The spectral variability of Swift J1644+57 in X-rays can be described by an irregular harder-when-brighter behavior tracking flares and dips, with a long term hardening trend associated with the decay phase. The harder-when-brighter behavior may arise from the interplay between the synchrotron spectral component and Comptonized radiation from the accretion disk. Our study of the duration, depth and dynamic range of the dips in the time interval from ∼14 to ∼405 days post-trigger confirm extreme variability of Swift J1644+57 throughout all the decay phase of the light curve.

This work was supported by NASA grant NNX10AK40G. This work made use of data supplied by the UK Swift Science Data Centre at the University of Leicester. We acknowledge the use of public data from the *Swift* data archive.

Facility: Swift

REFERENCES

Ayal, S., Livio, M., & Piran, T. 2000, ApJ, 545, 772
Barniol Duran, R. & Piran, T. 2013, ApJ, 770, 146
Barthelmy, S. D., Barbier, L. M., Cummings, J. R., et al. 2005, SSRv, 120, 143
Blandford, R. D. & Znajek, R. L. 1977, MNRAS, 179, 433
Bloom, J. S., Giannios, D., Metzger, B. D., et al. 2011, Science, 333, 203
Bogdanović, T., Eracleous, M., Mahadevan, S., Sigurdsson, S., & Laguna, P. 2004, ApJ, 610, 707
Bonnerot, C., Rossi, E. M., & Lodato, G. 2015, arXiv:1511.00300
Brassart, M. & Luminet, J. 2008, A&A, 481, 259
—. 2010, A&A, 511, A80+
Burrows, D. N., Hill, J. E., Nousek, J. A., et al. 2005, SSRv, 120, 165
Burrows, D. N., Kennea, J. A., Ghisellini, G., et al. 2011, Natur, 476, 421
Cannizzo, J. K. & Gehrels, N. 2009, ApJ, 700, 1047
Cannizzo, J. K., Lee, H. M., & Goodman, J. 1990, ApJ, 351, 38
Cannizzo, J. K., Troja, E., & Lodato, G. 2011, ApJ, 742, 32
Cash, W. 1979, ApJ, 228, 939
Celotti, A. & Ghisellini, G. 2008, MNRAS, 385, 283
Corral, A., Della Ceca, R., Caccianiga, A., et al. 2011, A&A, 530, A42
De Colle, F., Guillochon, J., Naiman, J., & Ramirez-Ruiz, E. 2012, ApJ, 760, 103
Evans, C., Laguna, P., & Eracleous, M. 2015, ApJL, 805, L19
Evans, P. A., Beardmore, A. P., Page, K. L., et al. 2009, MNRAS, 397, 1177
—. 2007, A&A, 469, 379
Fender, R. P., Belloni, T. M., & Gallo, E. 2004, MNRAS, 355, 1105
Gao, W.-H. 2012, ApJ, 761, 113
Gehrels, N. 1986, ApJ, 303, 336
Gehrels, N., Chincarini, G., Giommi, P., et al. 2004, ApJ, 611, 1005
Ghisellini, G. & Tavecchio, F. 2009, MNRAS, 397, 985
Giannios, D., & Metzger, B. D. 2011, MNRAS, 416, 2102
Gomboc, A. & Čadež, A. 2005, ApJ, 625, 278
Granot, J. & Sari, R. 2002, ApJ, 568, 820
Grupe, D., Burrows, D. N., Wu, X.-F., et al. 2010, ApJ, 711, 1008
Guillochon, J. & Ramirez-Ruiz, E. 2013, ApJ, 767, 25
—. 2015, ApJ, 809, 166
Guillochon, J., Ramirez-Ruiz, E., Rosswog, S., & Kasen, D. 2009, ApJ, 705, 844
Hayasaki, K., Stone, N. C., & Loeb, A. 2015, arXiv:1501.05207
Hayasaki, K., Stone, N., & Loeb, A. 2013, MNRAS, 434, 909
Kalberla, P. M. W., Burton, W. B., Hartmann, D., et al. 2005, A&A, 440, 775
Kawashima, T., Ohsuga, K., Usui, R., et al. 2013, PASJ, 65, L8
Kraft, R. P., Burrows, D. N., & Nousek, J. A. 1991, ApJ, 374, 344
Krimm, H. A., & Barthelmy, S. D. 2011, GRB Coordinates Network, 11891,
Krolik, J. H. & Piran, T. 2011, ApJ, 743, 134
Kumar, P., Barniol Duran, R., Bosnjak, Z., & Piran, T. 2013, MNRAS, 434, 3078
Kumar, P., Narayan, R., & Johnson, J. L. 2008, MNRAS, 388, 1729
Lacy, J. H., Townes, C. H., & Hollenbach, D. J. 1982, ApJ, 262, 120
Lei, W.-H., Zhang, B., & Gao, H. 2013, ApJ, 762, 98
Levan, A. J., Tanvir, N. R., Cenko, S. B., et al. 2011, Science, 333, 199
Lodato, G., King, A. R., & Pringle, J. E. 2009, MNRAS, 392, 332

Mangano, V., Burrows, D. N., Sbarufatti, B., & Cannizzo, J. K. 2014, Proceedings of Swift: 10 Years of Discovery (SWIFT 10), held 2-5 December 2014 at La Sapienza University, Rome, Italy. Online at http://pos.sissa.it/cgi-bin/reader/conf.cgi?confid=233, id.147, 147
Markwardt, C. B. 2009, in Astronomical Society of the Pacific Conference Series, Vol. 411, Astronomical Data Analysis Software and Systems XVIII, ed. D. A. Bohlender, D. Durand, & P. Dowler, 251
Massaro, E., Perri, M., Giommi, P., & Nesci, R. 2004, A&A, 413, 489
Metzger, B. D., Giannios, D., & Mimica, P. 2012, MNRAS, 420, 3528
Metzger, B. D., Piro, A. L., & Quataert, E. 2008, MNRAS, 390, 781
—. 2009, MNRAS, 396, 304
Protassov, R., van Dyk, D. A., Connors, A., Kashyap, V. L., & Siemiginowska, A. 2002, ApJ, 571, 545
Rees, M. J. 1988, Natur, 333, 523
Saxton, C. J., Soria, R., Wu, K., & Kuin, N. P. M. 2012, MNRAS, 422, 1625
Sbarufatti, B., Burrows, D. N., Gehrels, N., & Kennea, J. A. 2012, The Astronomer's Telegram, 4398, 1
Shen, R.-F. & Matzner, C. D. 2014, ApJ, 784, 87
Shiokawa, H., Krolik, J. H., Cheng, R. M., Piran, T., & Noble, S. C. 2015, ApJ, 804, 85
Stone, N., Sari, R., & Loeb, A. 2013, MNRAS, 435, 1809
Strubbe, L. E. & Quataert, E. 2009, MNRAS, 400, 2070
Tchekhovskoy, A., Metzger, B. D., Giannios, D., & Kelley, L. Z. 2014, MNRAS, 437, 2744
Tchekhovskoy, A., Narayan, R., & McKinney, J. C. 2010, ApJ, 711, 50
Vasudevan, R. V., Brandt, W. N., Mushotzky, R. F., et al. 2013, ApJ, 763, 111
Vercellone, S., Striani, E., Vittorini, V., et al. 2011, ApJL, 736, L38
Zauderer, B. A., Berger, E., Margutti, R., et al. 2013, ApJ, 767, 152
Zauderer, B. A., Berger, E., Soderberg, A. M., et al. 2011, Natur, 476, 425
Zdziarski, A. A., Ghisellini, G., George, I. M., et al. 1990, ApJL, 363, L1